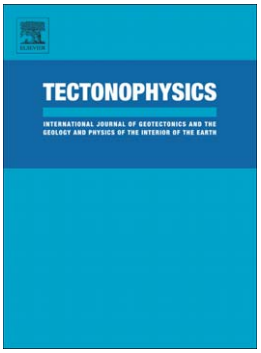

Accepted Manuscript

Inland extent of the Weddell Sea Rift imaged by new aerogeophysical data

Tom A. Jordan, Fausto Ferraccioli, Neil Ross, Hugh F.J. Corr, Philip T. Leat, Rob G. Bingham, David M. Rippin, Anne le Brocq, Martin J. Siegert

PII: S0040-1951(12)00568-9
DOI: doi: 10.1016/j.tecto.2012.09.010
Reference: TECTO 125612

To appear in: *Tectonophysics*

Received date: 3 December 2011
Revised date: 29 August 2012
Accepted date: 13 September 2012

Please cite this article as: Jordan, Tom A., Ferraccioli, Fausto, Ross, Neil, Corr, Hugh F.J., Leat, Philip T., Bingham, Rob G., Rippin, David M., le Brocq, Anne, Siegert, Martin J., Inland extent of the Weddell Sea Rift imaged by new aerogeophysical data, *Tectonophysics* (2012), doi: 10.1016/j.tecto.2012.09.010

This is a PDF file of an unedited manuscript that has been accepted for publication. As a service to our customers we are providing this early version of the manuscript. The manuscript will undergo copyediting, typesetting, and review of the resulting proof before it is published in its final form. Please note that during the production process errors may be discovered which could affect the content, and all legal disclaimers that apply to the journal pertain.

ACCEPTED MANUSCRIPT

Inland extent of the Weddell Sea Rift imaged by new aerogeophysical data

Tom A. Jordan[1*], Fausto Ferraccioli[1], Neil Ross[2], Hugh F.J. Corr[1], Philip T. Leat[1], Rob G. Bingham[3], David M. Rippin[4], Anne le Brocq[5], Martin J. Siegert[6]

[1]British Antarctic Survey, Madingley Road, Cambridge, U.K.

[2]School of Geography, Politics and Sociology, Newcastle University, U.K.

[3]School of Geosciences, University of Aberdeen, U.K.

[4] Environment Department, University of York, U.K.

[5] School of Geography, University of Exeter, U.K.

[6] Bristol Glaciology Centre, School of Geographical Sciences, University of Bristol, U.K.

* Corresponding author

e-mail: tomj@bas.ac.uk

Phone: +44 (0)1223 221305

Fax: +44 (0)1223 362616

ACCEPTED MANUSCRIPT

ACCEPTED MANUSCRIPT

Abstract

The Weddell Sea Rift was a major focus for Jurassic extension and magmatism during the early stages of Gondwana break-up and underlies the Weddell Sea Embayment, which separates East Antarctica from a collage of crustal blocks in West Antarctica. Newly-collected aerogeophysical data over the catchments of Institute and Möller ice streams reveal the inland extent of the Weddell Sea Rift against the Ellsworth-Whitmore block and a hitherto unknown major left-lateral strike slip boundary between East and West Antarctica. Aeromagnetic and gravity anomalies define the regional subglacial extent of Proterozoic basement, Middle Cambrian rift-related volcanic rocks, Jurassic intrusions and sedimentary rocks of inferred post-Jurassic age. 2D and 3D magnetic depth-to-source estimates were used to help constrain joint magnetic and gravity models for the region. The models reveal that Proterozoic crust similar to that exposed at Haag Nunataks, extends southeast of the Ellsworth Mountains to the margin of the Coastal Basins. Thick granitic Jurassic intrusions are modelled at the transition between the Ellsworth-Whitmore block and the thinner crust of the Weddell Sea Rift and within the Pagano Shear Zone. The crust beneath the inland extension of the Weddell Sea Rift is modelled as being either ~4 km thinner compared to the adjacent Ellsworth-Whitmore block or as underlain by an up to 8 km thick mafic underplate.

Highlights

- Boundaries between the Weddell Sea Rift, West Antarctica, and East Antarctia.
- Geophysical data images a major fault zone separating East and West Antarctica.
- Proterozoic basement, Cambrian volcanic rocks, Jurassic granites are mapped.
- Deep crustal underplate underlies Jurassic granites, not upper crustal mafic rocks.

Keywords: Continental rifting, Strike-slip faulting, aeromagnetic, gravity, Antarctica

ACCEPTED MANUSCRIPT

1 Introduction

The Weddell Sea Embayment (Fig. 1) lies within the region where Gondwana breakup initiated by Jurassic rifting of Antarctica and Africa (Dalziel et al., 2000; Elliot and Fleming, 2000; Storey et al., 2001). The embayment extends for 1200 km from the Orion Anomaly to the Ellsworth Whitmore Mountains (EWM) and is ~700 km wide (Golynsky et al., 2000). A collage of four micro-plates form West Antarctica and lie west and south of the Weddell Sea Embayment: the Antarctic Peninsula, Thurston Island, Marie Byrd Land, and the EWM (Dalziel and Elliot, 1982). In East Antarctica, the embayment in flanked by the Coats Land block, the Shackleton Range and the Dufek Intrusion (Fig. 1) (Studinger and Miller, 1999). The Weddell Sea Embayment therefore lies in a key position for understanding the structural relationship between East and West Antarctica, and the development of continental rifting processes during the early stages of Gondwana break-up.

The tectonic history of Weddell Sea Embayment is hotly debated. The EWM block, is inferred from structural and paleomagnetic data to have been located adjacent to South Africa within Gondwana (Curtis, 2001; Randall and MacNiocaill, 2004) and subsequently displaced from Africa to West Antarctica during Jurassic rifting ~180 Ma (Dalziel, 2007; Dalziel and Grunow, 1992). Alternatively, palaeomagnetic results have been interpreted as revealing later mid-Cretaceous (~100 Ma) block motion along a shear zone in the Weddell Sea region (DiVenere et al., 1996). The hypothesis for significant (~1000 km) post-Jurassic motion within the Weddell Sea Embayment, is however incompatible with reconstructions of marine magnetic anomalies north of the Orion anomaly (Ghidella et al., 2007). Additionally, more recent models of South Atlantic and SW Indian ocean evolution do not require major

ACCEPTED MANUSCRIPT

movements of West Antarctic micro-plates during Gondwana breakup (Eagles and Vaughan, 2009).

Evidence for continental rifting and associated magmatism in the Weddell Sea Embayment derives from reconnaissance geophysical data and geological investigations. Regional gravity data have been modelled as indicating that the Weddell Sea Rift is underlain by ~27 km thick rifted continental crust; in addition a Te (effective elastic thickness) of ~35 km has been estimated for the region, suggesting that continental rifting may have occurred in a period between 230-160 Ma (Studinger and Miller, 1999). Seismic data at the edge of Filchner and Ronne Ice shelves suggest high stretching factors between 1.5 and 3.0 (Hübscher et al., 1996; Jokat et al., 1996). Large-scale bimodal Middle Jurassic magmatism has been linked to a Jurassic superplume plume in the Weddell Sea Embayment region (Storey and Kyle, 1997; Storey et al., 2001), which has been suggested to have heralded early Gondwana break-up (Riley and Knight, 2001; Storey, 1995; Storey et al., 2001; White and McKenzie, 1989). Both the layered mafic Dufek Intrusion and the dolerite sills and Kirkpatrick Basalts of the Ferrar Large Igneous Province of East Antarctica (Elliot and Fleming, 2000; Elliot et al., 1999; Leat, 2008) and Jurassic granites exposed in the EWM (Storey et al., 1988) have been related to Weddell Sea rifting processes.

Recent satellite gravity data suggest that the thinned continental crust of the Weddell Sea Rift continues inland towards the margin of the EWM block (Block et al., 2009). However, our ability to analyse Mesozoic continental rifting processes and associated magmatism onshore has been hampered by the paucity of near surface geophysical exploration (e.g. Behrendt 1974; Garrett et al., 1988; Storey et al., 1988). Widely spaced radar and aeromagnetic surveys were flown in the 70's and 80's over the region, and limited oversnow radar, seismic and land

ACCEPTED MANUSCRIPT

gravity traverse data was acquired in 1950's and 1960's (Behrendt et al., 1974; Thiel, 1961). We present recently acquired airborne radar, aeromagnetic and aerogravity data that provide a new view of subglacial geology and crustal structure inland of the Weddell Sea Rift and enable us to identify a previously unknown major strike-slip fault system separating East and West Antarctica.

2 Geological and geophysical framework

2.1 Pre-Jurassic rocks

Aeromagnetic data indicate that highly magnetic Proterozoic basement similar to that exposed in the Haag Nunataks (Fig. 1) (Millar and Pankhurst, 1987; Storey et al., 1994) underlies part of the EWM (Garrett et al., 1987; Maslanyj and Storey, 1990), which includes a ~13 km thick succession of folded Cambrian to Permian age metasediments (Curtis and Storey, 1996; Storey et al., 1988). The metasedimentary sequence contains volcanic rocks and intrusive sills up to 300 m thick (Fig. 2a), interpreted to have formed in a Middle Cambrian continental rift setting (Curtis et al., 1999; Vennum et al., 1992).

The metasediments in the EWM are unaffected by the Cambrian-Ordovician Ross Orogen indicating that this block was not in its present position relative to East Antarctica at ~500 Ma (Curtis and Storey, 1996; Storey and Dalziel, 1987). The entire stratigraphic succession was affected by two post-Permian stages of deformation (Curtis, 2001). The main dextral transpressive Permo-Triassic deformation event within the Ellsworth Mountains (Fig. 2a) suggests that the EWM was part of the South African Cape Fold Belt (Curtis and Storey, 1996). Palaeomagnetic reconstructions support the interpretation that the EWM block was

ACCEPTED MANUSCRIPT

adjacent to South Africa prior to early Gondwana break-up (Randall and MacNiocaill, 2004). Two structural domains have been proposed for the EWM region: the Ellsworth Domain to the west, and the more highly deformed Marginal Domain to the east (Storey and Dalziel, 1987).

2.2 Jurassic rifting and magmatism

Gravity data reveal thinned continental crust beneath the Filchner Rift and Weddell Rift Anomaly (Aleshkova et al., 2000; Studinger and Miller, 1999) (Fig. 1). Seismic refraction data image crustal thinning beneath the Filchner Rift and additionally indicate extensive mafic underplating (Leitchenkov and Kudryavtzev, 2000), likely related to Jurassic rifting processes and possibly to an inferred mantle plume in the Weddell Sea Embayment. A 'rift-rift-rift' triple junction may have developed during an early phase of Gondwana breakup, with the failed third arm of the rift extending along the Central Trough (Ferris et al., 2002; Ferris et al., 2000).

Jurassic igneous rocks are exposed along the flanks of the Weddell Sea Embayment and are inferred from geophysical data within the embayment. A Jurassic volcanic rifted margin appears to flank East Antarctica (Hunter et al., 1996; Leitchenkov et al., 1996). The Explora magnetic anomaly is interpreted as arising from a Mid-Jurassic seaward dipping volcanic sequence (Hinz and Krause, 1982; Hunter et al., 1996) or Jurassic intrusions associated with the Filchner Rift (Golynsky et al., 2000; Leitchenkov and Kudryavtzev, 2000). The Explora Anomaly may link to the exposed mafic-ultramafic Dufek intrusion (Behrendt et al., 1980; Ferris et al., 1998), which is part of the Jurassic Ferrar Large Igneous Province (Minor and Mukasa, 1997). Jurassic granites intrude Palaeozoic metasediments (Fig. 2a) within the

ACCEPTED MANUSCRIPT

EWM block and are dated by Rb-Sr methods at 176-173 Ma (Storey et al., 1988). The granites have S-type affinity, with 70 to 76 % wt.% SiO_2, similar to other post-tectonic granites (Vennum and Storey, 1987b) and may have been derived from mafic Ferrar-like magma (Storey et al., 1988). At Hart Hills a sheared quartz-gabbro that exhibits geochemical similarities with the Ferrar suite intrudes deformed metasedimentary rocks (Storey et al., 1988; Vennum and Storey, 1987a). Positive aeromagnetic anomalies over exposures of the Jurassic granites have been interpreted as revealing 5-10 km mafic bodies beneath the granites (Garrett et al., 1988).

3 Aerogeophysical survey

3.1 Survey layout and procedures

An extensive aerogeophysical survey was undertaken over the catchments of the Institute and Möller ice streams during the 2010/11 field season (Fig. 2b). Approximately 23,000 km of aerogeophysical data were collected during 27 flights, covering an area of ~209,000 km^2. Operations were from two field camps, first C110 for 17 flights, then Patriot Hills for 10 flights (Fig. 2b). A favourable weather window, with low wind and relatively clear skies allowed completion of all survey flights between 23th December and 12th January. The survey aircraft was a British Antarctic Survey (BAS) Twin Otter, equipped with airborne radar, aeromagnetic, airborne gravity, and laser altimeter systems, configured to allow simultaneous collection of all data streams. Technical capabilities of the radar, magnetic and gravity systems were as reported previously (Corr et al., 2007; Ferraccioli et al., 2007a; Jordan et al., 2007), and the swath laser system is similar to that reported by (Hvidegaard et al., 2011). The main survey grid was flown at 7.5 km line spacing with tie lines every 25 km.

ACCEPTED MANUSCRIPT

Exploratory lines (with a 50 km spacing) were also flown to link to previous aerogeophysical surveys over the West Antarctic Rift System (Bell et al., 1998; Blankenship et al., 2001; Ferraccioli et al., 2007b; Studinger et al., 2002; Vaughan et al., 2006) and the Dufek intrusion (Ferris et al., 2003).

The survey was flown in four constant elevation blocks (Fig. 2b) to facilitate collection of aerogravity data while not exceeding the ~500 m surface clearance limit, above which the radar data may become degraded. The changes in altitude at block boundaries lead to inevitable loss of ~25 km of airborne gravity data. Data loss was minimised by re-flying the overlapping sections, where possible. The 'stepped' flight pattern also ensured line intersections were at the same elevation, simplifying magnetic levelling procedures. Flights generally coincided with periods of minimal diurnal magnetic disturbance as measured at the local magnetic base station, between ~14:00 and 01:00 UTC.

Positional information was calculated from GPS (Global Positioning System) and IMU (Inertial Measurement Unit) data. Two Leica 500 GPS base stations were operated at the field camp throughout the survey, and Leica 500 and Novatel DL-V3 GPS receivers were fitted in the aircraft. In addition an iMAR® IMU was fitted directly beneath the gravity meter. Data were processed using the Novatel Inertial Explorer post processing software. We used a 'loosely coupled' approach where first kinematic GPS solutions were calculated between a single Leica base station and the Novatel GPS receiver, before INS data were integrated. Positional data were referenced to WGS-84 ellipsoidal heights. The second GPS base station and receiver were run for backup. The reported standard deviation on the positional error for the GPS kinematic solutions was 7 cm in the horizontal and 20 cm in the vertical dimension.

ACCEPTED MANUSCRIPT

The loosely coupled positional solutions, including the IMU data, showed reduced errors with a standard deviation of 4.1 cm horizontal and 6.5 cm vertical.

3.2 Subglacial topography

Previous knowledge of the subglacial topography beneath the Institute and Möller Ice Streams (Fig. 1) derived from reconnaissance airborne radar data flown in the 1970s by the SPRI/NSF/TUD programme (Drewry, 1983), and limited airborne radar data collected in the 1980s by BAS (Garrett et al., 1988). Line spacing was ~50 km, and ice thickness was often not recovered. Additionally, positioning for the 1970s surveys typically relied on inertial navigation systems and reckoning, which can introduce significant positional errors of 2-3 km (Garrett et al., 1988; Jankowski and Drewry, 1981).

Our new ice penetrating radar data were collected using a coherent system with a carrier frequency of 150 MHz, a bandwidth of 12 MHz (Corr et al., 2007; Ross et al., 2012). To yield an enhanced view of the ice-bed interface we applied Doppler processing that helps focus radar-scattering hyperbola in the along-track direction. With a 13 Hz data rate we obtain a ~10 m along track sampling interval. The onset of the received bed echo was picked using PROMAX seismic processing software and yielded a crossover RMS error of ~18 m (Ross et al., 2012). Bedrock elevation was interpolated onto a 2.5 km grid mesh using a minimum curvature algorithm.

Our airborne radar data reveal the detailed bedrock topography of the Institute and Möller Ice Stream region (Fig. 3a). The northern part of the area is dominated by two broad basins herein named the Coastal Basins up to 1800 m below sea level (Ross et al., 2012). The

ACCEPTED MANUSCRIPT

Southern Basin may represent the onshore continuation of the Thiel Trough that lies between Berkner Island and the Dufek Intrusion (TT in Fig. 1) (Drewry, 1983).

The Ellsworth Trough incises the Ellsworth Whitmore Mountains and reaches depths of >2000 m below sea level. A complex series of en-echelon basins (Fig 3a), marks the transition between the Ellsworth and Marginal domains (Storey and Dalziel, 1987); we define these as the Transitional Basins. The en-echelon basins are between 40 and 80 km long and 10 to 20 km wide. Northeast of Hart Hills, closed, elongate basins are recognised, which we call the Marginal Basins. The most elevated topography corresponds to the EWM, where we mapped peak elevations between 1100 and 2293 m.

3.3 Magnetic anomalies

To obtain the aeromagnetic anomalies we applied magnetic compensation, IGRF removal, base station diurnal correction, statistical levelling and microlevelling. Magnetic compensation was carried out using the using the PEICOMP program from Pico Envirotec, and other processing steps were carried out using Geosoft™ Oasis Montage 7.3© software. Prior to base station correction, the data had a cross-over error standard deviation of 62 nT. Our magnetic base station was located at C110 for the first half of the survey and at Patriot Hills for the second half of the survey, with flights extending up to 487 km from the base (Fig. 2b). Errors associated with large base station separation (Maslanyj and Damaske, 1986) were minimised by low-pass filtering base station observations (Damaske, 1989). The cross-over error standard deviation was 46.6 nT after the base station correction. Statistical levelling was then applied to minimise residual heading errors and shorter wavelength diurnal variations. The levelled data were draped to 2100 m above the bed topography (the average bed clearance) using a 2D Fourier method (Pilkington and Thurston, 2001). The draped

ACCEPTED MANUSCRIPT

magnetic data were then interpolated onto a grid with a 750 m cell size (1/10 line spacing), and micro-levelling was applied to minimise residual flight line corrugation (Ferraccioli et al., 1998). After statistical and microlevelling the final RMS error was 4 nT. The final stage in data processing was reduction to the pole (RTP), using an inclination and declination of -69.6° and 43.1° respectively. Power spectra analysis shows that anomalies with wavelengths of ~3km can be resolved from our draped magnetic line data.

3.3.1 Reduced to the pole magnetic anomaly map

The map of RTP aeromagnetic anomalies (Fig. 3b) shows a broad correlation with subglacial topography. Three of the positive magnetic anomalies correspond to exposures of Jurassic granite at Pirrit Hills, Nash Hills and Pagano Nunataks as noted in previous reconnaissance aeromagnetic surveys (Garrett et al., 1988). The Pirrit Hills anomaly has an amplitude of up to 290 nT and wavelength of ~50 km. The Nash Hills anomaly has a similar overall wavelength of ~50 km, but lower amplitude of ~60 nT. The E-W trending Pagano Anomaly has an amplitude of up to 246 nT and is ~50 km wide. It extends ~125 km towards the coast from Pagano Nunatak and is flanked by the Transitional and Marginal Basins. Magnetic lineaments (L1-L5) broadly correspond to the main subglacial topographic trends. The Ellsworth Anomalies (EA) are located between the Ellsworth Mountains and the Ellsworth Trough and exhibit amplitudes of ~40 nT and wavelengths of ~20 km. M1 is a ~40 km wide anomaly with an amplitude of 95 nT and is located adjacent to the Western Basin. The EA and anomaly M1 are inferred to reflect Cambrian volcanics and Proterozoic basement rocks respectively, as discussed further in Section 7.1. Within the Coastal Basin magnetic anomalies are generally subdued. Anomalies M2 and M3 have amplitudes of ~20 nT and a

ACCEPTED MANUSCRIPT

wavelength of ~50 km. They are bounded by E-W trending lineations L2, L3 and L4 that flank the northern margin of the Transitional Basins. Minor positive magnetic anomalies are located between the M2 and the Pagano Anomaly and correspond to the margins of some of the en-echelon basins. Anomalies M4, M5 and M6, between Nash Hills and the Pagano Anomaly are approximately circular positive anomalies with wavelengths of ~30 km and amplitudes between 20 and 40 nT. Much higher amplitude (>450 nT) and short wavelength anomalies are superimposed on a broader magnetic low over the Whitmore Mountains. We interpret these anomalies as reflecting Cenozoic rift-related magmatism along the flank of the West Antarctic Rift System (Behrendt et al., 2004).

3.4 Gravity anomalies

3.4.1 Aerogravity data processing

The airborne gravity data were processed using Geosoft Oasis Montage 7.3 software. Dynamic corrections related to aircraft movement were derived from differential GPS and inertial navigation data, processed using Waypoint™ Inertial-Explorer software (Kennedy et al., 2007). Corrections to the raw airborne gravity data were made for vertical acceleration, the first order Eötvos effect (Harlan, 1968), horizontal accelerations (LaCoste, 1967), latitude on the WGS 84 ellipsoid (Woollard, 1979) and elevation above WGS 84 ellipsoid (linear free air correction of 0.3086 mGal/m). We do not correct our data to the geoid, as it is poorly known in this region. The variations in the measured gravity field are therefore strictly gravity disturbances (Hackney and Featherstone, 2003). However, for consistency with the geophysical literature the local variations in gravity field associated with geological sources are referred to hereafter as gravity anomalies. Relative gravity anomalies were drift

ACCEPTED MANUSCRIPT

corrected, and tied back to the absolute gravity value at Rothera Station (Jones and Ferris, 1999) using a LaCoste and Romberg land gravity meter. After these corrections were applied, the data were filtered with a 9 km ½ wavelength space-domain kernel filter to minimise short wavelength noise (Holt et al., 2006). Microlevelling techniques can also be applied to gravity data to minimise residual line to line noise remaining after standard levelling procedures (Ferraccioli et al., 2011; Lane, 2004). We applied Butterworth filtering and directional cosine filtering to microlevel the data (Ferraccioli et al., 1998). The maximum and minimum of the microlevelling correction was 4.45 and -3.63 mGal, with a standard deviation of 1.24 and mean of 0 mGal. The microlevelled free air gravity data were upward continued (Pilkington and Thurston, 2001) to a uniform altitude of 2600 m, corresponding to the highest flight elevation of the survey. The final cross-over RMS error was 4.3 mGal, which is slightly higher than the ~3 mGal of previous Antarctic airborne gravity surveys (Bell et al., 1999; Ferraccioli et al., 2006; Jones et al., 2002; Jordan et al., 2010). We attribute this to the stepped pattern of the tie-line flights, which meant that only shorter lengths of tie-line data could be used.

3.4.2 Free air and Bouguer anomaly maps

The free air gravity anomaly (Fig. 4a) shows a clear correlation with the subglacial topography (Fig. 3a). Maximum positive values of 50 to 60 mGal are observed towards the EWM, and the plateau region close to the centre of the survey area has mean value of -7 mGal. Negative values of ~-75 mGal are recorded across the Coastal Basins, and within the Transitional Basins. Minimum anomalies of -85 to -95 mGal are recorded across the Ellsworth Trough and on a single regional line towards the Whitmore Mountains.

ACCEPTED MANUSCRIPT

The Complete Bouguer gravity anomaly was calculated to reveal the subsurface geological structure and regional crustal thickness variation (Fig. 4b). The 3D gravity effect due to the ice/air and ice/rock interfaces were calculated using a 3D fast Fourier transform method (Parker, 1973) at a uniform observation altitude of 2600 m. Assumed ice and rock densities were 917 kgm^{-3} and 2670 kgm^{-3} respectively. To ensure that shorter wavelength noise was not introduced we filtered the Bouguer correction with same low-pass filter applied to the raw free air data (9 km ½ wavelength space-domain kernel filter). Topographic data were extended a minimum of 165 km from the gravity flights, allowing the computation of a fully terrain-corrected Bouguer gravity anomaly, equivalent to Hayford zone O.

Errors in sub-ice topography will introduce noise into the Bouguer correction. The reported RMS bedrock elevation error of ~18 m from the radar data would introduce an error of ~2mGal. However, the error in sub-ice topography is significantly lower (<1mGal) at the ~20 km wavelengths relevant to correction of the airborne gravity data. We did not include in the Bouguer correction a water column beneath the floating ice shelf to the north of the survey area as this is poorly known. Our parameter tests show that assuming a 1000 m water column in place of ice < 1mGal of error would result at a distance of ~18 km from the coast.

The gridded Bouguer anomaly shows values of >40 mGal over the Coastal Basins, and negative values ~-100 mGal towards the EWM. Such variation in the Bouguer anomaly is likely associated with crustal thickness variations. Additional negative Bouguer anomalies of 20 to 40 mGal and wavelength of ~50 km coincide with the exposed Jurassic granites and associated positive magnetic anomalies. Magnetic anomalies M2 and M4-M6 are also linked with local Bouguer negatives. In contrast, magnetic anomaly M1 is not associated with a negative Bouguer anomaly.

ACCEPTED MANUSCRIPT

4 Aeromagnetic data enhancement

4.1 Short and long wavelengths

To investigate tectonic structures and subglacial geology in further detail, we applied a variety of digital enhancement techniques to the aeromagnetic data. These enhancements were limited to the region covered by the higher resolution grid. Regional geological structures were enhanced using the 10 km upward continued magnetic anomaly map (Fig. 5a).Upward continuation was carried out using a fast Fourier transform technique (Blakely, 1995). The main magnetic lineaments (L1-L5) are not significantly smoothed out compared to the RTP data indicating that these features likely represent major structural boundaries. Additionally, the anomalies associated with the exposed Jurassic granites and anomalies M2 and M4-M6 are still present, indicating that these are likely caused by thick source bodies. In contrast, the western end of anomaly M3 is significantly attenuated, indicating a likely relatively shallower and thinner source body. A long wavelength negative magnetic anomaly is apparent between the Coastal Basins and Pirrit Hills.

Shorter wavelength anomalies associated with shallower structures were enhanced by subtracting the upward continued anomaly grid from the initial RTP anomaly grid (Fig. 5b). Anomalies M2 and M3 are enhanced as are the anomalies associated with Jurassic granitic intrusions and anomalies M4-M6. Additionally, it becomes apparent that the EA is formed by a series of shorter wavelength anomalies, approximately parallel to L1. Other short wavelength anomalies (M7 and M8) and lineation L6, which show the same trend as the EA,

ACCEPTED MANUSCRIPT

become more apparent between the EA and anomaly M2. The Coastal Basins remain magnetically quiet suggesting a lack of shallow magnetic sources over the region.

4.2 Derivatives and magnetic lineations

The edges of the major magnetic source bodies and structural lineations can be enhanced by calculating the maximum horizontal gradient of pseudo-gravity (Fig. 6a) (Blakely and Simpson, 1986; Cordell and Grauch, 1985). An automated algorithm was used to detect all peaks within the pseudo-gravity field to locate the edges of the sources (Blakely and Simpson, 1986) and the main lineations were then manually picked. Lineations L1-L6 and within EA are all recovered by this technique. Additionally, the margins of the main positive magnetic anomalies associated with the Jurassic granite outcrops, and the margins of anomalies M4 and M6 are also located.

To further enhance the magnetic signal we calculated the tilt angle of the RTP magnetic anomaly grid (Fig. 6b) (Cooper and Cowan, 2006; Miller and Singh, 1994). The tilt angle responds equally well to shallow and deep sources and to a large dynamic range of amplitudes for sources at the same level and therefore enhances subtle low amplitude anomalies. The tilt angle locates the peaks of the anomalies outlined by the maximum horizontal gradient of pseudo-gravity. The extent of anomalies M2 and M3 are however more clearly defined. The NW-SE trending EA and the series of approximately parallel anomalies to the south, noted in the residual filtered data (Fig. 5b) are also apparent, and appear to be truncated by anomaly M2. Peaks in the tilt derivative field were calculated (Blakely and Simpson, 1986) and the key lineations manually picked.

ACCEPTED MANUSCRIPT

An alternative method to locate anomaly margins and enhance lineations is the normalised maximum horizontal gradient amplitude (TDX) (Fig. 6c), which gives high values over anomaly margins (Cooper and Cowan, 2006). This enhancement is relatively insensitive to the depth of the source body, and therefore improves the definition of shallow magnetic sources. By applying a threshold value of 0.0004 we isolated the anomaly margins. The margins of the Pirrit and Nash Hills magnetic anomalies are well defined. The linear flanks of the Pagano Anomaly are also imaged parallel to L5. The margins of anomalies M4-6 are also recognised as approximately circular structures. Between anomaly M2 and the Ellsworth Anomaly a generally consistent trend is observed, approximately parallel to the main topographic grain of the Ellsworth Mountains and lineation L6 is highlighted. Between M2 and the Pagano Anomaly a complex pattern of short discontinuous anomaly margins are suggested, with no clear regional trend. Over the Marginal Basins fewer TDX peaks are recovered, which show a structural grain approximately parallel the Pagano Anomaly.

4.3 Apparent and measured magnetic susceptibility

Aeromagnetic data can be compared to measured rock properties by transforming the observed magnetic anomaly to apparent susceptibility (Blakely, 1995; Cordell and Grauch, 1985). Our apparent susceptibility map (Fig. 6d), calculated from the RTP anomalies, assumes the tops of the source bodies are coincident with the ice/bed interface. The results of this calculation therefore provide minimum estimates of rock susceptibility. If the top of the magnetic sources were deeper a higher susceptibility would be required. We compared the computed apparent susceptibility values with measurement of magnetic susceptibility held by the Polar Rock Repository at Byrd Polar Research Center, Ohio State University (Table 1).

ACCEPTED MANUSCRIPT

Over anomaly M1 the estimated susceptibility is ~8x10^{-3} SI units. This is higher than any values measured in the Ellsworth Mountains, or in the local nunataks, but is comparable to the values measured over the Proterozoic gneiss exposed in the Haag Nunataks (Flowerdew et al., 2007; Garrett et al., 1987; Millar and Pankhurst, 1987; Storey et al., 1994). The lower amplitude Ellsworth Anomaly has an apparent susceptibility of 1-2 x10^{-3} SI, which would be consistent with the values measured in mafic Cambrian igneous rocks within the Ellsworth Mountains (Curtis et al., 1999). Higher apparent susceptibilities of 12-20 x10^{-3} SI are calculated over the Pirrit Hills and Pagano Anomalies. These are an order of magnitude larger than measured susceptibility in the exposed Jurassic granites.

5 Depth to magnetic source calculation

To help constrain the depth and geometry of the magnetic source bodies we applied 3D Euler and a range of 2D magnetic depth to source techniques (Figs 7 and 8). The 3D Euler deconvolution method (Reid et al., 1990) returns a series of solutions for set window sizes and assumed structural indexes (source geometry). We chose an 8.75 km window (5X5 grid cells) and assumed a structural index SI=1, which can be used to detect edges of sill and dyke like bodies and faults. A 5x5 window is generally adequate to detect shallower sources from magnetic datasets and the edges of the source bodies derived from our 3D Euler clusters are in good agreement with anomaly margins picked with the TDX technique.

The 2D techniques applied included Analytical Signal (Nabighian, 1972), Werner deconvolution (Ku and Sharp, 1983) and Extended Euler deconvolution (Mushayandebvu et al., 2001; Reid et al., 1990) (Fig 7 c-g and Fig 8 b-f). These techniques use the gradient of the

ACCEPTED MANUSCRIPT

magnetic field along a profile within a specified window and assumptions about the source body to provide source depth estimates. Data were sampled every 250 m from the final microlevelled magnetic anomaly grid. To remove gridding artefacts, a 6.75 km low pass filter was applied to the magnetic data before calculation of the gradients. Solutions were limited to be between the bed and 14 km depth. We analysed both dyke solutions (or small throw fault) and contact solutions (or large throw fault). Results from Analytical Signal and Werner Deconvolution were calculated for incremental windows between 5 and 15 km wide, corresponding to the approximate wavelength of the magnetic gradient. After calculation, Analytical and Werner solutions were clustered to help focus spray patterns and further constrain the results. Clustering was done in Oasis Montage™ and gave the average solution within a 1.5 by 1.5 km window, if more than 5 solutions were present. Solutions for Extended Euler Deconvolution assumed a fixed window of 5 km. Our Extended Euler results showed few spray patterns, when a limit of 10% discrepancy between Euler and Extended Euler techniques was imposed; solutions for this technique were therefore not clustered. We compared 3D and 2D depth to source results for two regions: the Nash Hills and the Pagano Anomaly region (Fig 7) and the Coastal Basins region (Fig. 8).

5.1 The inland profile

3D Euler Deconvolution returns predominately well clustered shallow depth solutions around the Nash Hills region (Fig. 7a). The locations of these solutions are close to the anomaly margins picked by the TDX enhancement, and flank the magnetic high in this area. This area of shallow solutions overlies a negative Bouguer anomaly. Anomalies M4 and M6 (Fig. 7b) show similar patterns of depth solutions to Nash Hills, with predominately shallow depth to

ACCEPTED MANUSCRIPT

source solutions. The depth to source solutions for the Pagano Anomaly are more complex, with shallow solutions dominating along the southern flank of the anomaly, while deep solutions are noted to the north. This pattern would be consistent with a northward dipping body as the source of the Pagano Anomaly.

The profile over Nash Hills and the Pagano Anomaly shows the main magnetic anomalies (Fig. 7c) generally correlate with subglacial highlands (Fig. 7d). The 2D Analytical Signal method (Fig. 7e) shows both dyke and contact solutions. Shallow Analytical solutions are returned beneath the Nash Hills area (consistent with 3D Euler results), extending to a depth of >12 km. However, the deeper solutions are likely spray patterns. Anomaly M5 is associated with Analytical solutions ~ 5 km deep. Anomaly M4 and the Pagano Nunataks anomaly show intermediate solutions between ~4 km and the surface. The Werner technique (Fig. 7e) gives a range of solutions between ~3 and ~8 km depth, mostly concentrated towards the northern and southern ends of the profile. The 2D Euler method (Fig. 7f) shows clusters of solutions close to the ice/bed interface in Nash Hills. Similar strong clusters of solutions are associated with the Pagano Nunatak anomaly, though these cluster 1 to 4 km beneath the bed, suggesting a deeper source body. The M5 anomaly, at the centre of the profile, is associated with a shallow cluster of Euler solutions, suggesting the top of this body is within ~2 km of the bed. Although all techniques produce broadly similar results, with shallow sources over the main anomalies, the results along this profile demonstrate the variability in depth recovered by different inversion techniques.

ACCEPTED MANUSCRIPT

5.2 The coastal profile

The coastal profile crosses both the Coastal Basins and the Transitional Basins (Fig. 8). 3D Euler solutions show a series of clusters in this region, which broadly coincide with magnetic anomaly margins defined by TDX (Fig. 8a). The crest of anomaly M1 shows a series of shallow 3D Euler solutions, indicating a source close to the ice-bed interface. Within the Coastal Basins clusters of deep 3D Euler solutions are observed. To the west of the Coastal Basins shallow 3D Euler solutions are noted.

2D Analytical signal solutions also show solutions extending almost to the ice-bed interface beneath anomaly M1 (Fig. 8d). Across the centre of the basin a few deep (>10 km) analytical solutions are detected, before a series 4-5 km deep solutions are recorded coincident with anomaly M3. A series of shallower solutions ~3km deep are found beneath the Transitional Basins adjacent to lineations L3 and L4, which mark the margins of anomaly M1. Werner solutions (Fig. 8d) across the Coastal Basin are generally shallower than Analytical signal results. The shallowest Werner solutions are close to anomaly M1. Fewer Werner solutions are found in the centre of the basin between 1 and 4 km beneath the ice/bed interface, and a group of solutions are found at the edge of the M3 anomaly at ~5km depth. Euler solutions (Fig. 8e) show a broadly similar pattern to the Analytical solutions with the shallowest results close to M1 ~1km beneath the ice/rock interface and few deep results (11-13 km deep) in the centre of the basin. Shallow (~1 km) clusters of solutions are associated with anomaly M3, with the shallowest solutions beneath the Transitional Basins area.

6 Forward modelling

ACCEPTED MANUSCRIPT

Two dimensional crustal models were constructed using GM-SYS® magnetic and gravity modelling software (Talwani and Ewing, 1960). The 2D magnetic depth-to-source estimates discussed previously were superimposed to provide an initial guide for our models. Magnetic and Bouguer gravity anomalies were both modelled with the aim of analysing intra-crustal features such as Jurassic intrusions, basement features, sedimentary basin extent and depth to Moho. Models considered the geometry of the upper crustal structures and explored two alternative scenarios for crustal thickness variation, with and without mafic underplating (the latter to account for seismic evidence offshore - see Leitchenkov et al., 1996 and Section 8.3). A horizontal boundary between the upper and lower crust was imposed at 15 km depth in all models. This interface was included to account for the assumed increase in density between the upper and lower crust. A depth of 15 km was chosen as it is below the upper crustal structures, above the crust-mantle boundary, and approximately coincides with the 'Conrad Discontinuity' noted in continental seismic studies (Litak and Brown, 1989). The horizontal orientation of this interface means that it does not create any gravity trend or anomaly.

6.1 Inland Profile

Three distinct magnetic anomalies in the Nash Hills area are modelled as being caused by a ~8 km thick magnetic igneous body, with low susceptibility 'roof pendants' of country rock at its top surface (Fig. 9a). The presence of roof pendants is consistent with local geological observations (Storey et al., 1988). The modelled magnetic susceptibility of the source rock was 7.6 x10^{-3} SI (Table 2), i.e. an order of magnitude higher than the measured susceptibility (Table 1). Our modelling implies that the magnetisation of the exposed granites is not representative of the bulk magnetic properties of the underlying intrusive source body. The

ACCEPTED MANUSCRIPT

Pagano Anomaly and the M4 and M5 anomalies are modelled as similar intrusive source bodies between 6 and 10 km thick, with susceptibilities shown in Table 2. Increasing the apparent magnetic susceptibilities would reduce the thickness of the modelled bodies. However, in order to simultaneously fit the gravity lows larger negative density contrasts would be required.

Gravity modelling is generally insensitive to the absolute depth of the Moho and helps reveal the relative change in crustal thickness. For the gravity model we assumed an initial crustal thickness of 30 km. A thickness of 27 km was estimated from seismic refraction and spectral analysis of gravity data for the Ronne Ice Shelf area (Fig 1) (Studinger and Miller, 1999). A ~3 km relative increase in crustal thickness inland can account for the observed inland decrease in Bouguer gravity anomaly from the Weddell Sea. Densities assumed for mantle and lower crust are shown in Table 2 and followed previous models for the Weddell Sea Embayment region (Studinger and Miller, 1999).

The Bouguer anomaly on the inland profile shows a general increasing trend from EWM to East Antarctica and a gravity high (B1) in the area of the Transitional Basins, which we fit by introducing crustal thinning to ca 28 km beneath the basins. A quiet magnetic anomaly signature corresponds to the area of B1 between magnetic anomalies M5 and M4 and was modelled by introducing sedimentary infill in the Transitional Basins. Negative Bouguer anomaly B2 is explained by the deeper lower density intrusion I2.

The observed 20-50 km wavelength negative Bouguer anomalies B3 and B4 correlate with positive magnetic anomalies and exposures of Jurassic granite at Nash Hills and Pagano Nunatak (Fig. 9a). Granitic rocks have a wide density range of 2500-2810 kgm^{-3} (Telford et al., 1990). Assuming a minimum density of 2500 kgm^{-3} the minimum thickness for the

ACCEPTED MANUSCRIPT

granitic source body in the Nash Hills region is 5.6 km. A higher density of 2550 kgm^{-3} would suggest a granitic body ~8.5 km thick. The modelled intrusions appear to lie at the lower end of the density range typical of granitic rocks, which is reasonable given that the outcropping granites have high SiO_2 (70-75 wt. %) and K-feldspar rich compositions (Vennum and Storey, 1987b). Applying a density of 2550 kgm^{-3} to all the magnetic bodies on the inland profile generally provided a good match to the observed Bouguer gravity anomalies (Fig. 9a).

6.2 Coastal Profile

Along the Coastal Profile (Fig. 9b) the magnetic source body for anomaly M1 was modelled as a high susceptibility basement block (C1), based on the high apparent magnetic susceptibility (see also Fig. 6d). Clusters of depth to source solutions close to the bed suggested a shallow top of C1. A good fit for the transition between M1 and the magnetically quiet Coastal Basins was obtained by extending the flanks of C1 to depths of over 10 km. Clusters of Werner solutions within the Coastal Basins at ~3.5 km depth are interpreted as the base of an inferred sedimentary basin (S). Depth solutions beneath anomaly M3 locate the top of intrusive body C2 ~2.5 km below the bed. The thickness of the intrusion is ~1 km, assuming an apparent magnetic susceptibility and density contrast similar to the intrusions along the inland profile.

Our gravity models show that the regional trend in the Bouguer anomaly can be accounted for by assuming a ~4 km step in crustal thickness towards the Ellsworth Mountains. We also assumed that basement block C1 has a higher apparent density of 2700 kgm^{-3}, relative to the upper crustal metasediments. Bouguer anomaly B5 overlies the Coastal Basins and is modelled as reflecting ~2 km thick sedimentary infill (S). An apparent density of 2500 kgm^{-3}

ACCEPTED MANUSCRIPT

created a ~-8 mGal anomaly, which is close to what is observed. Assuming Airy isostatic compensation a~2 km thick sedimentary infill would yield ~1 km of additional crustal thinning. A lower density of 2300 kgm^{-3}, as inferred for sediments beneath the Ronne Ice Shelf (Aleshkova et al., 2000), was also tested. However, this resulted in a larger negative anomaly of >20 mGal. Tests showed that sedimentary infill between 1 and 3 km thick could fit the gravity data equally well, with minor modifications to density and crustal thickness.

6.3 Alternative gravity models including magmatic underplating

Our starting gravity models discussed above assume a 27-30 thick crust for the inland extent of the Weddell Sea Rift and a standard crust-mantle density contrast (Studinger and Miller, 1999). However, a shallower Moho depth of ~24 km has been inferred onshore from a single seismic reflection point (see Fig. 2a for location) (Behrendt et al., 1974). Additionally, widespread magmatic underplating has been seismically imaged at the margins of the Ronne Ice Shelf (Leitchenkov and Kudryavtzev, 2000). Hence we computed two alternative gravity models for the inland and coastal profile, assuming a thinner crust and an anomalous high density underplated layer at the crust-mantle interface (Fig. 10). In the alternative models we assumed that the upper crustal structure was the same as shown in Figure 9. Bouguer anomaly B1 on the inland profile can be modelled by assuming a ~8 km thick high density body at the base of the crust interpreted as magmatic underplating (Fig. 10a). Along the coastal profile the modelled underplated body is less extensive and only ~3 km thick, and the Moho has greater relief (Fig. 10b).

ACCEPTED MANUSCRIPT

7 Interpretation

A new geological sketch map of the inland margin of the Weddell Sea Rift was compiled based on a combination of aeromagnetic, gravity and geological data and forms the basis to discuss the subglacial geology and tectonic architecture of the region (Fig. 11).

7.1 Proterozoic basement and Cambrian rift-related igneous rocks

The broad magnetic low over the EWM reflects the over 10 km thick Paleozoic metasedimentary sequences as previously modelled from reconnaissance aeromagnetic data (Fig.10 in (Maslanyj and Storey, 1990)). Permian-Triassic folds and faults within the exposed metasediments trend ~NNW-SSE in the northern Ellsworth Mountains and NW-SE in the southern Ellsworth Mountains (Curtis, 2001). The NW-SE structural grain has also been mapped at Pirrit and Nash Hills in the Ellsworth Domain (Storey and Dalziel, 1987). The dominant magnetic lineations we observe have an ESE-WNW orientation (Fig. 11a and Fig. 11b2). These lineations may reflect Permo-Triassic transpressional deformation structures and/or basement structural grain.

Magnetic anomalies M1, EA and anomalies M7 and M8 are interpreted as revealing Proterozoic basement and Cambrian rocks (Fig. 11c). Highly magnetic and dense Proterozoic basement similar to the gneissic basement exposed in the Haag Nunataks (Flowerdew et al., 2007; Garrett et al., 1987; Millar and Pankhurst, 1987; Storey et al., 1994) is interpreted as the source of magnetic anomaly M1. The southward increase in stratigraphic age along the Ellsworth Mountains (Curtis, 2001) and the petrology of Cambrian igneous exposed rocks in the Ellsworth Mountains (Curtis et al., 1999) support our interpretation for Late Proterozoic basement of the EWM. The higher frequency EA, M7 and

ACCEPTED MANUSCRIPT

M8 magnetic anomalies trace the subglacial extent of Cambrian rift-related igneous rocks that outcrop within the Ellsworth Mountains (Curtis et al., 1999; Vennum et al., 1992).

7.2 Jurassic intrusions

Previous models of the magnetic anomalies within the EWM region predicted that ~5-10 km thick Jurassic granites with low susceptibility were underlain by 10-12 km thick mafic intrusions (Garrett et al., 1988). However, our magnetic depth to source solutions suggest that the intrusive bodies that cause the anomalies are significantly shallower (Figs 7 and 8) and our gravity models do not require the presence of underlying mafic intrusions (see also discussion). The exposed granites in both the Ellsworth and Marginal domains have been dated to between 173 and 175 Ma and appear to be undeformed (Storey et al., 1988). However, at Hart Hills sheared quartz-gabbro has been reported (Vennum and Storey, 1987a). We note that the circular magnetic highs and gravity lows typical of the Pirrit Hills and Nash Hills region differ from the more elongate magnetic highs and gravity lows at the transition between the Ellsworth and Marginal Domains. It is possible therefore that different suites of Jurassic intrusions are present with the more elongate intrusions being emplaced along a major fault zone, as we discuss in the following section.

7.3 The Pagano Shear Zone

Structural observations within the Marginal Domain reveal dominant NE-SW trends within highly deformed Paleozoic metasediments, which is normal to structural trends within the Ellsworth Domain (Storey and Dalziel, 1987). The Transitional Basins and their flanking

ACCEPTED MANUSCRIPT

highlands represent the most remarkable topographic features of the Marginal Domain region (Fig. 3a). Magnetic anomalies M2-M3 and the Pagano Anomaly lie north of the Marginal Domain and are interpreted as reflecting Jurassic intrusions. Our rose diagram shows that magnetic lineations within this region have a dominant ~E-W trend and a subsidiary ~ENE trend (Fig 11 b3). These magnetic lineations directions are interpreted as reflecting faults and the margins of Jurassic intrusions. By analysing these magnetic lineations we propose several alternative kinematic interpretations for the regional stress field. Using detailed maps and profiles of the topography and magnetic anomalies we interpreted the location and orientation of structural boundaries and intrusions in the Transitional Basins region (Figure 12). The Transitional Basins have a right-stepping en-echelon pattern that is typical of strike-slip fault systems (Reading, 1980). We propose that the E-W magnetic trends image the Principal Displacement Zone of the strike-slip fault system with the ENE trends reflecting synthetic shears and the NE-SW trends representing normal faults. As shown in Figure 11 b4 our magnetic interpretation is compatible with the pattern of faulting and the strain ellipse for left-lateral strike-slip fault systems (Lodolo et al., 2003; Reading, 1980). There is a close spatial relationship between the Pagano Anomaly and the inferred strike-slip fault system. Our preferred interpretation predicts that the boundary between the Ellsworth Domain and the Marginal Domain is represented by the left-lateral Pagano Shear Zone, which in turn controlled the location of the Jurassic intrusions (Fig. 11c).

Magnetic lineament analysis alone does not provide definitive structural geological interpretations or kinematic solutions. The limitations in using aeromagnetic data for structural analysis include difficulties in gleaning information from non-magnetic rock packages and the non-uniqueness of geological source characterisation through magnetic imaging and modelling (Betts et al., 2003). Consequently, alternative interpretations of fault

ACCEPTED MANUSCRIPT

zones based on aeromagnetic imaging are often presented (Ferraccioli and Bozzo, 2003). We put forward two possible alternative interpretations for the tectonic boundary between the Ellsworth and Marginal domains. The first one predicts that the NE-SW magnetic trends reflect Permo-Triassic or older basement grain of the Marginal Domain as opposed to synthetic left-lateral shear zones. The E-W oriented magnetic grain appears to truncate the NE-SW magnetic fabric (e.g. Fig. 12b) and could represent an extensional fault zone that became leaky facilitating the emplacement of Jurassic intrusions. However, this would require ~N-S oriented extension that is rotated ~90° compared to the E-W oriented extension previously suggested with the southern Weddell Sea Rift (Ferris et al., 2000), see also Section 8.1). The second alternative is that both the NE-SW and the E-W magnetic trends are imaging normal faults related to NW-SE and N-S oriented extension directions. These alternative scenarios cannot be ruled out but would require a more complex triaxial strain regime at the southern end of the Weddell Sea rift, which may be akin to the rift-rift-rift triple junction model suggested at the northern end of the Weddell Sea Rift (Ferris et al., 2000).

7.4 The Coastal Basins

Magnetic depth to source solutions and gravity and magnetic models lead us to interpret the Coastal Basins as underlain by ~2 km of low density sedimentary rock (Fig. 9b). The smooth bed within the Coastal Basins (Ross et al., 2012) supports our interpretation for sediments in the region (see also Fig 13 g). To assess the location and orientation of structural boundaries in the Coastal Basins region we show detailed maps and profiles of the topography and magnetic anomalies in Figure 13. The maps reveal that the Western and Southern basin margins have distinct N-S and E-W trends. The N-S trend is parallel to rift fabric within the

ACCEPTED MANUSCRIPT

Weddell Sea Rift (see Section 8.1). The E-W trend corresponds to the orientation of the Pagano Shear Zone (Fig 11 b). The age of the sediments modelled within the Coastal Basins is not known. However, rifting is typically followed by thermal subsidence, and the deposition of sediments in a passive margin setting (Royden and Keen, 1980; White and McKenzie, 1988). We therefore suggest the modelled sediments in the Coastal Basins post-date Jurassic rifting, as proposed also for sediments imaged beneath the Ronne Ice Shelf (Studinger and Miller, 1999).

8 Discussion

We combined our aerogravity and aeromagnetic data with adjacent gravity and magnetic datasets and with satellite gravity data to discuss tectonic and magmatic features of the Weddell Sea Rift (Fig. 14).

8.1 Inland extent of the Mesozoic Weddell Sea Rift

Our new airborne gravity data reveal the inland extent of the Mesozoic Weddell Sea Rift. The N-S orientation of the positive Bouguer anomaly we mapped beneath the Coastal Basins region is similar to the southern part of the Weddell Rift gravity Anomaly (Aleshkova et al., 2000) (Fig. 14a). According to our 2D gravity models the inland extent of the Weddell Sea Rift features ~4 km of crustal thinning compared to the adjacent EWM region (Fig. 9b). We see no evidence for a connection between the inland extent of the Mesozoic Weddell Sea Rift and the Mesozoic to Cenozoic West Antarctic Rift System (Dalziel, 2006). The combination of our airborne gravity, satellite gravity (Pail et al., 2010) and a single land gravity traverse

ACCEPTED MANUSCRIPT

(Behrendt et al., 1974) clearly reveals the boundary between the inland extent of the Weddell Sea Rift and East Antarctica. The ~E-W trend of the boundary is particularly clear from satellite gravity data (Fig 14b) and appears to lie on strike with the trend of the inferred Pagano Shear Zone. N-S oriented magnetic trends are well defined within the Weddell Sea Rift (Fig. 14c) (Golynsky et al., 2000) and lie on strike with the trends we identified along the flanks of the Western Basin (Fig 13b) . This supports our interpretation of the inland extent of the Mesozoic Weddell Sea Rift in the Coastal Basins region. The inferred Pagano Shear Zone however lies at high angle to the Weddell Sea rift fabric as previously noted.

8.2 Pagano Shear Zone and the boundary between East and West Antarctica.

Our preferred interpretation of the Pagano Shear Zone has important geodynamic implications for tectonic reconstructions of the Weddell Sea region that have not considered the possibility of a major left-lateral strike-slip system within the region. The magnetic trends within the Weddell Sea Rift have been interpreted as resulting from either basement blocks bounded by extensional rift-related fault systems (Ferris et al., 1998; Golynsky et al., 2000) and/or Jurassic intrusions (Ferris et al., 2000; Golynsky et al., 2000). Additionally, aeromagnetic interpretations along the edge of East Antarctica, in the region between Berkner Island and the Dufek Intrusion, suggested the existence of a ~N-S oriented dextral strike-slip Jurassic fault system and a ~E-W oriented normal fault system (Figs. 14d and 15). However, in our preferred interpretation the E~W trends represent the continuation of the left-lateral Pagano Shear Zone in the Thiel Trough region.

We consider two alternative kinematic interpretations for the southern edge of the Weddell Sea Rift and for the boundary between East and West Antarctica. In the simple shear model

ACCEPTED MANUSCRIPT

~E-W oriented extension within the Filchner Rift is accomodated by left-lateral strike-slip motion on the Pagano Shear Zone (Fig. 16a). The shear zone would enable eastward motion of the EWM block relative to East Antarctica, which is permissible given that a variety of geological and paleomagnetic reconstructions have indicated that the EWM is a micro-plate that was displaced from an original pre-Gondwana break-up position closer to East Antarctica (Curtis and Storey, 1996; Randall and MacNiocaill, 2004). In the more complex pure shear model the sinistral and dextral faults are conjugate fault systems (Fig. 16b). A pure shear system would however imply a more NW-SE oriented extension in the Weddell Sea Rift and NE-SW oriented compression in the hinge zone between the strike-slip fault systems. Field and experimental studies over V-shaped conjugate strike-slip faults suggest that the simple shear and pure shear cases are likely be to be end-member models and that more complex non-coaxial fault patterns are likely (Yin and Taylor, 2011).

8.3 Jurassic granites and magmatic underplating hypothesis

We have interpreted ~circular Jurassic intrusions as emplaced at the transition between the thicker crust of the EWM and the inland extent of the Weddell Sea Rift and more elongated structurally-controlled intrusions along the flanks of the Pagano Shear Zone (Fig 11c). Petrological and geochemical studies indicate that the exposed Jurassic granites have geochemical affinities with an enriched mantle-derived mafic-ultramafic magma source similar to the Ferrar LIP and exhibit a degree of crustal contamination (Storey et al., 1988). Rift-related granites are often associated with mafic magmatism. For example, during the breakup of Rodinia granitic magmatism was coeval with mafic magmatism along the margins of the Congo Craton (Tack et al., 2001) and in China (Li et al., 2003). Along the Cretaceous

ACCEPTED MANUSCRIPT

rifted margin of Namibia exposed granites have been linked to underlying gabbroic rocks imaged by magnetic, gravity and seismic data (Bauer et al., 2003). In the case of the granites at inland edge of the Weddell Sea Rift significant uncertainties surround the existence, location and depth of the hypothesised mafic magma sources. Previous interpretations of aeromagnetic data suggested that the Jurassic granites are directly underlain by >10 km thick mafic intrusions in the upper crust (Garrett et al., 1988), which could speculatively provide the inferred mafic source required by the geochemical data. However, the aeromagnetic anomalies we observed differ from the much higher amplitude anomalies detected over the Dufek mafic-ultramafic intrusion (Ferris et al., 1998; Ferris et al., 2003) and the higher frequency anomalies over the thin Ferrar sills (Ferraccioli et al., 2009a; Ferraccioli et al., 2009b; Shepherd et al., 2006). From a more general perspective, magnetic anomaly patterns per se do not require mafic source rocks. Magnetic susceptibility patterns of granitic rocks are determined by their bulk chemistry and magnetic mineralogy. Around the world, the values reported for magnetic susceptibility in granites range widely from 10^{-6} [SI] in leucocratic granites up to 10^{-1} [SI] in some granodiorites and tonalities (Gregorová et al., 2003). The Saruhan granites in Turkey provide an example of zoning pattern of magnetic susceptibility across the plutons with the highest values of magnetic susceptibility in the center. The most differentiated rock types have high SiO2 content and low magnetic susceptibility and exposed are at the rim of the intrusions (Aydın et al., 2007). We infer that the weakly magnetic exposed Jurassic granites of the Ellsworth and Marginal domains may exhibit similar zoning with a more magnetic ferrimagnetic granitic core. Our gravity models (Fig. 9) do not require high density intrusions in the upper crust, which generally image mafic intrusions (Telford et al., 1990). The 20 to 40 mGal negative Bouguer anomalies we observed over the Jurassic intrusions differ from the positive Bouguer anomalies observed, for example, over Jurassic

ACCEPTED MANUSCRIPT

alkaline intrusions of the Jutulstraumen rift, which have been interpreted to be underlain by ~10 km thick mafic intrusions (Ferraccioli et al., 2005). The negative Bouguer anomalies we observed are more comparable to those typically observed over several km-thick granite plutons elsewhere in the world (Améglio and Vigneresse, 1999; Taylor, 2007; Zeng et al., 2000). In the Permian age Oslo rift, joint interpretation of petrophysical, magnetic, gravity and seismic data have been used to propose that thin granitic intrusions are underlain by ~10 km thick mafic intrusions with no associated positive Bouguer gravity anomaly (Ebbing et al., 2007). The lack of gravity signature of the mafic intrusions inferred beneath the Olso Rift is due to the anomalously dense upper crust (Ebbing et al., 2007). A similar scenario may be possible also for the edge of the EWM, which are inferred to be underlain at least in part by Proterozoic basement (that could be anomalously dense). However, the lack of independent geophysical and geological constraints makes this alternative scenario difficult to either validate or refute.

We explored a simpler scenario in our gravity models, which involves mafic to ultramafic magmatic underplating at the base of the crust beneath the exposed Jurassic granites. Our modelling revealed that with a flat Moho assumption the thickness of the underplated layer beneath the Ellsworth and Marginal Domains is ~8 km. In contrast, assuming ~4 km of crustal thinning beneath the Coastal Basins region a ~3 km thick layer of magmatic undeplating is modelled (Fig. 10). Seismic velocities associated with underplated mafic rocks at the Greenland margin (Voss and Jokat, 2007) and in Namibia (Bauer et al., 2003) are comparable to those imaged at the front of the Ronne Ice Shelf, where extensive magmatic underplating has also been interpreted (Leitchenkov and Kudryavtzev, 2000). If magmatic underplating does continue inland beneath our study region then it would extend ~900 km from the outer edge of the Ronne Ice Shelf to the EWM. The hypothesis for widespread

ACCEPTED MANUSCRIPT

magmatic underplating is attractive as it could provide a thermal source for partial melting of the EWM crust and the missing mafic magma source required to explain the geochemical signatures of the Jurassic granites (Storey et al., 1988). However, independent constraints on crustal thickness and lower crustal and upper mantle seismic velocities are required to test the viability of the magmatic underplating hypothesis further.

9 Conclusions

We have presented a new integrated aerogeophysical dataset including airborne radar, aeromagnetic, and aerogravity data that shed new light on the inland extent of the Mesozoic Weddell Sea Rift in Antarctica. A combination of digital enhanced aeromagnetic maps, coupled with depth to magnetic source and joint magnetic and gravity models, enabled us to map the subglacial geology and deeper crustal structure of the region. Specifically, we interpreted the data to compile a new geological sketch map portraying the subglacial extent of Proterozoic basement, Cambrian volcanic and Permo-Triassic metasedimentary rocks, Jurassic intrusions, and inferred post-Jurassic sedimentary infill in the Coastal Basins. Our structural interpretation, based on the analysis of magnetic patterns and lineations, reveals a hitherto unknown major fault zone that we call the Pagano Shear Zone. The proposed left-lateral shear zone forms a regional tectonic boundary between the Ellsworth and Marginal domains, and likely represents a major fault separating the EWM block in West Antarctica from East Antarctica. We also infer that the Pagano Shear Zone may have facilitated the emplacement of Jurassic intrusions and accommodated southwards motion of the EWM block during the Jurassic opening of the Weddell Sea Rift. Our gravity modelling provides no support for previously inferred upper crustal mafic intrusions beneath the Jurassic granites of

ACCEPTED MANUSCRIPT

the EWM region. Although the mafic underplating hypothesis would adequately explain the geochemical evidence from the Jurassic granites, the airborne geophysical data alone cannot differentiate the crustal thinning and underplating hypothesises. Seismic investigations are required to provide independent constraints on crustal thickness and magmatic underplating.

Acknowledgements

We wish to thank British Antarctic Survey for logistical support, and Antarctic Logistics and Expeditions (ALE) for input of the fuel for the survey. In particular we wish to thank Ian Potten the pilot for the airborne survey and Carl Robinson for his survey equipment engineering work and support. We also wish to thank Anne Grunow from the Polar Rock Repository at Byrd Polar Research Center, Ohio State University, for magnetic susceptibility data and discussion about regional geology. We gratefully acknowledge Emanuele Lodolo and Theresa Diehl for their helpful and constructive reviews of the paper and thank Alan Vaughan for further suggestions on structural interpretations. Funding for this project was provided by the UK NERC AFI grant NE/G013071/1.

ACCEPTED MANUSCRIPT

ACCEPTED MANUSCRIPT

References

Aleshkova, N.D., Golynsky, A.V., Kurinin, R.G., Mandrikov, V.S., 2000. Gravity mapping in the Southern Weddell Sea Region. (Explanatory note for free-air and Bouguer anomalies maps). Polarforschung 67, 163-177.

Améglio, L., Vigneresse, J.L., 1999. Geophysical imaging of the shape of granitic intrusions at depth: a review, in: Castro, A. (Ed.), Understanding Granites: Integrating New and Classical Techniques. Geological Society, London, Special Publications, pp. 39-54.

Aydın, A., Feré, E.C., Aslan, Z., 2007. The magnetic susceptibility of granitic rocks as a proxy for geochemical composition: Example from the Saruhan granitods, NE Turkey. Tectonophysics 441, 85-95.

Bauer, K., Trumbull, R.B., Vietor, T., 2003. Geophysical images and a crustal model of intrusive structures beneath the Messum ring complex, Namibia. Earth and Planetary Science Letters.

Behrendt, J.C., Blankenship, D.D., Morse, D.L., Bell, R., 2004. Shallow source aeromagnetic anomalies observed over the West Antarctic Ice Sheet compared with coincident bed topography from radar ice sounding - New evidence for glacial "removal" of subglacially erupted Late Cenozoic rift related volcanic edifices. Global and Planetary Change 42, 177-193.

Behrendt, J.C., Drewry, D.J., Jankowski, E.J., Grim, M.S., 1980. Aeromagnetic and Radio Echo Ice-Sounding Measurements Show Much Greater Area of the Dufek Intrusion, Antarctica. Science 209, 1014-1017, DOI: 1010.1126/science.1209.4460.1014

Behrendt, J.C., Henderson, J.R., Meister, L., Rambo, W.L., 1974. Geophysical investigations of the Pensacola Mountains and adjacent glacierized areas of Antarctica.

ACCEPTED MANUSCRIPT

Bell, R., Blankenship, D.D., Finn, C.A., Morse, D.L., Scambos, T.A., Brozena, J.M., Hodge, S.M., 1998. Influence of subglacial geology on the onset of a West Antarctic ice stream from aerogeophysical observations. Nature 394, 58-62.

Bell, R.E., Childers, V.A., Arko, R.A., Blankenship, D.D., Brozena, J.M., 1999. Airborne gravity and precise positioning for geologic applications. Journal of Geophysical Research 104, 15281-17292.

Betts, P.G., Giles, D., Lister, G.S., 2003. Tectonic environment of shale-hosted massive sulphide Pb-Zn-Ag deposits of Proterozoic northeastern Australia. Economic Geology 98, 557-576.

Blakely, R.J., 1995. Potential Theory in Gravity and Magnetic Applications. Cambridge University Press, Cambridge.

Blakely, R.J., Simpson, R.W., 1986. Approximating edges of source bodies from magnetic or gravity anomalies. Geophysics 51, 1494-1498.

Blankenship, D.D., Morse, D.L., Finn, C., Bell, R., Peters, M.E., Kempf, S.D., Hodge, S.M., Studinger, M., Behrendt, J.C., Brozena, J.M., 2001. Geologic controls on the initiation of rapid basal motion for the West Antarctic ice streams: a geophysical perspective including new airborne radar sounding and laser altimetry results., in: Alley, R.B., Bindschadler, R.A. (Eds.), The West Antarctic Ice Sheet: behaviour and environment, pp. 105–121.

Block, A.E., Bell, R., Studinger, M., 2009. Antarctic crustal thickness from satellite gravity: Implications for the Transantarctic and Gamburtsev Subglacial Mountains. Earth and Planetary Science Letters 288, 194-203.

Cooper, G.R.J., Cowan, D.R., 2006. Enhancing potential field data using filters based on the local phase. Computers & Geosciences 32, 1585-1591.

ACCEPTED MANUSCRIPT

Cordell, L.E., Grauch, V.J.S., 1985. Mapping basement magnetization zones from aeromagnetic data in the San Juan Basin, New Mexico, in: Hinze, W.J. (Ed.), The utility of regional gravity and magnetic anomaly maps. Soc. Explor. Geophys.,, pp. 181-197.

Corr, H., Ferraccioli, F., Frearson, N., Jordan, T.A., Robinson, C., Armadillo, A., Caneva, G., Bozzo, E., Tabacco, I.E., 2007. Airborne Radio-Echo Sounding of the Wilkes Subglacial Basin, the Transantarctic Mountains, and the Dome C Region, in: Bozzo, E., Ferraccioli, F. (Eds.), The Italian–British Antarctic Geophysical and Geological Survey in Northern Victoria Land 2005–06—Towards the International Polar Year 2007–08. Terra Antartica Reports, pp. 55-63.

Curtis, M.L., 2001. Tectonic history of the Ellsworth Mountains, West Antarctica: Reconciling a Gondwana enigma. Geol. Soc. Am. Bull. 113, 939-958.

Curtis, M.L., Leat, P.T., Riley, T.R., Storey, B.C., Millar, I.L., Randall, D.E., 1999. Middle Cambrian volcanism in the Ellsworth Mountains: Implications for paleo-Pacific margin tectonics. Tectonophysics 304, 275-299.

Curtis, M.L., Storey, B.C., 1996. A review of geological constraints on the pre-break-up position of the Ellsworth Mountains within Gondwana: implications for Weddell Sea evolution, in: Storey, B.C., King, E.C., Livermore, R.A. (Eds.), Weddell Sea Tectonics and Gondwana Break-up. Geological Society Special Publication, pp. 11-30.

Dalziel, I.W.D., 2006. On the Extent of the Active West Antarctic Rift System. Terra Antarctica 12, 193-202.

Dalziel, I.W.D., 2007. The Ellsworth Mountains: Critical and enduringly enigmatic, in: Cooper, A.K., Raymond, C.F. (Eds.), Antarctica: A Keystone in a Changing World – Online Proceedings of the 10th ISAES. USGS Open-File Report 2007-1047, Short Research Paper 004, 5 p.; doi:10.3133/of2007-1047.srp004.

ACCEPTED MANUSCRIPT

Dalziel, I.W.D., Elliot, D.H., 1982. West Antarctica: problem child of Gondwanaland. Tectonics 1, 3-19.

Dalziel, I.W.D., Grunow, A., 1992. Late Gondwanide tectonic rotations within Gondwanaland. Tectonics 11, 603-606.

Dalziel, I.W.D., Lawver, L., Murphy, J.B., 2000. Plumes, orogenesis, and supercontinental fragmentation. Earth and Planetary Science Letters 178, 1-11.

Damaske, D., 1989. Geomagnetic Activity and its Implications for the Aeromagnetic Survey in North in: Damaske, D., Dürbaum, H.J. (Eds.), German Antarctic North Victoria Land Expedition 1984/85. Schweizerbart'sche Verlagsbuchhandlung, Stuttgart, pp. 41-56.

DiVenere, V.J., Kent, D.V., Dalziel, I.W.D., 1996. Summary of palaeomagnetic results from West Antarctica: implications for the tectonic evolution of the Pacific margin of Gondwana during the Mesozoic, in: Storey, B.C., King, E.C., Livermore, R.A. (Eds.), Weddell Sea Tectonics and Gondwana Break-up. Geological Society, London, Special Publications pp. 31-43.

Drewry, D.J., 1983. Antarctica: glaciological and geophysical folio. University of Cambridge. Scott Polar Research Institute., Cambridge.

Eagles, G., Vaughan, A.P.M., 2009. Gondwana breakup and plate kinematics: Business as usual. Geophysical Research Letters 36, doi:10.1029/2009GL037552.

Ebbing, J., Skilbrei, J.R., Olsen, O., 2007. Insights into the magmatic architecture of the Oslo Graben by petrophysically constrained analysis of the gravity and magnetic field. Journal of Geophysical Research 112, doi:10.1029/2006JB004694.

Elliot, D.H., Fleming, T.H., 2000. Weddell triple junction: The principal focus of Ferrar and Karoo magmatism during initial breakup of Gondwana. Geology 28, 539-542, doi: 510.1130/0091-7613(2000)1128<1539:WTJTPF>1132.1130.CO;1132.

ACCEPTED MANUSCRIPT

Elliot, D.H., Fleming, T.H., Kyle, P.R., Foland, K.A., 1999. Long-distance transport of magmas in the Jurassic Ferrar large igneous province, Antarctica. Earth and Planetary Science Letters 167, 89-104.

Ferraccioli, F., Armadillo, A., Jordan, T.A., Bozzo, E., Corr, H., 2009a. Aeromagnetic exploration over the East Antarctic Ice Sheet: a new view of the Wilkes Subglacial Basin. Tectonophysics 478, 62-77, doi:10.1016/j.tecto.2009.1003.1013.

Ferraccioli, F., Armadillo, A., Zunino, A., Bozzo, E., Rocchi, S., Armienti, P., 2009b. Magmatic and tectonic patterns over the Northern Victoria Land sector of the Transantarctic Mountains from new aeromagnetic imaging. Tectonophysics 487, 43-61, doi:10.1016/j.tecto.2008.1011.1028

Ferraccioli, F., Bozzo, E., 2003. Cenozoic strike-slip faulting from the eastern margin of the Wilkes Subglacial Basin to the western margin of the Ross Sea Rift: an aeromagnetic connection, in: Storti, F., Holdsworth, R.E., Salvini, F. (Eds.), Intraplate Strike-Slip Deformation Belts. The Geological Society of London Special Publication pp. 109-133.

Ferraccioli, F., Finn, C., Jordan, T.A., Bell, R.E., Anderson, L.M., Damaske, D., 2011. East Antarctic rifting triggers uplift of the Gamburtsev Mountains. Nature 479, 388-392, doi:310.1038/nature10566.

Ferraccioli, F., Gambetta, M., Bozzo, E., 1998. Microlevelling procedures applied to regional aeromagnetic data: an example from the Transantarctic Mountains (Antarctica). Geophysical Prospecting 46, 177-196, DOI: 110.1046/j.1365-2478.1998.00080.x.

Ferraccioli, F., Jones, P.C., Curtis, M.L., Leat, P.T., 2005. Subglacial imprints of early Gondwana break-up as identified from high resolution aerogeophysical data over western Dronning Maud Land, East Antarctica. Terra Nova 17, 573–579.

ACCEPTED MANUSCRIPT

Ferraccioli, F., Jones, P.C., Vaughan, A.P.M., Leat, P.T., 2006. New aerogeophysical view of the Antarctic Peninsula: More pieces, less puzzle. Geophysical Research Letters 33, doi:10.1029/2005GL024636.

Ferraccioli, F., Jordan, T.A., Armadillo, A., Bozzo, E., Corr, H., Caneva, G., Robinson, C., Frearson, N., Tabacco, I.E., 2007a. Collaborative aerogeophysical campaign targets the Wilkes Subglacial Basin, the Transantarctic Mountains and the Dome C region, in: Bozzo, E., Ferraccioli, F. (Eds.), The Italian–British Antarctic Geophysical and Geological Survey in Northern Victoria Land 2005–06—Towards the International Polar Year 2007–08. Terra Antartica Reports, pp. 1-36.

Ferraccioli, F., Jordan, T.A., Vaughan, D.G., Holt, J.W., James, P.R., Corr, H., Blankenship, D.D., Fairhead, J.D., Diehl, T.M., 2007b. New aerogeophysical survey targets the extent of the West Antarctic Rift System over Ellsworth Land, in: Cooper, A.K., Raymond, C.R. (Eds.), Antarctica: A Keystone in a Changing World –Online Proceedings of the 10th ISAES X. USGS, p. 4.

Ferris, J.K., Johnson, A.C., Storey, B.C., 1998. Form and extent of the Dufek intrusion, Antarctica, from newly compiled aeromagnetic data Earth and Planetary Science Letters 154, 185-202

Ferris, J.K., Storey, B.C., Vaughan, A.P.M., Kyle, P.R., Jones, P.C., 2003. The Dufek and Forrestal intrusions, Antarctica: A centre for Ferrar Large Igneous Province dike emplacement? Geophysical Research Letters 30, doi:10.1029/2002GL016719.

Ferris, J.K., Vaughan, A.P.M., King, E.C., 2002. A window on West Antarctic crustal boundaries: the junction between the Antarctic Peninsula, The Filchner Block, and the Weddell Sea oceanic lithosphere. Tectonophysics 347, 13-23.

ACCEPTED MANUSCRIPT

Ferris, J.K., Vaughan, A.P.M., Storey, B.C., 2000. Relics of a complex triple junction in the Weddell Sea embayment, Antarctica. Earth and Planetary Science Letters 178, 215-230.

Flowerdew, M.J., Millar, I.L., Curtis, M.L., Vaughan, A.P.M., Horstwood, M.S.A., Whitehouse, M.J., Fanning, C.M., 2007. Combined U-Pb geochronology and Hf isotope geochemistry of detrital zircons from early Paleozoic sedimentary rocks, Ellsworth-Whitmore Mountains block, Antarctica. Geol. Soc. Am. Bull. 119, doi: 10.1130/B25891.25891.

Garrett, S.W., Herrod, L.D.B., Mantripp, D.R., 1987. Crustal structure of the area around Haag Nunataks, West Antarctica: new aeromagnetic and bedrock elevation data. , in: McKenzie, G.D. (Ed.), Gondwana Six: Structure, Tectonics and Geophysics. American Geophysical Union Geophysical Monograph, pp. 109-116.

Garrett, S.W., Maslanyj, M.P., Damaske, D., 1988. Interpretation of aeromagnetic data from the Ellsworth Mountains-Thiel Mountains ridge, West Antarctica. Journal of the Geological Society (London) 145, 1009-1017.

Ghidella, M.E., Lawver, L., Gahagan, L.M., 2007. Break-up of Gondwana and opening of the South Atlantic: Review of existing plate tectonic models, in: Cooper, A.K., Raymond, C.F. (Eds.), Antarctica: A Keystone in a Changing World – Online Proceedings of the 10th ISAES. USGS Open-File Report 2007-1047, pp. 5 p.; doi:10.3133/of2007-1047.srp3055.

Golynsky, A., Chiappini, M., Damaske, D., Ferraccioli, F., Ferris, J.K., Finn, C., Ghidella, M.E., Isihara, T., Johnson, A., Kim, H.R., Kovacs, L., LaBrecque, J., Masolov, V., Nogi, Y., Purucker, M., Taylor, P., Torta, M., 2001. ADMAP – Magnetic Anomaly Map of the Antarctic, 1:10 000 000 scale map, in: Morris, P., von Frese, R.R.B. (Eds.), BAS (Misc) 10. British Antarctic Survey, Cambridge.

ACCEPTED MANUSCRIPT

Golynsky, A.V., Grikurov, G.E., Kamenev, E.N., 2000. Geological significance of regional magnetic anomalies in Coats Land and Western Dronning Maud Land. Polarforschung 67, 91-99.

Gregorová, D., Hrouda, F., Kohút, M., 2003. Magnetic susceptibility and geochemistry of Variscan West Carpathian granites: implications for tectonic setting. Physics Chemistry Earth 28, 729-734.

Hackney, R.I., Featherstone, W.E., 2003. Geodetic versus geophysical perspectives of the gravity anomaly. Geophysical Journal International 154, 35-43.

Harlan, R.B., 1968. Eotvos corrections for airborne gravity. Journal of Geophysical Research 73, 4675 - 4679.

Hinz, K., Krause, W., 1982. The continental margin of Queen Maud Land, Antarctica: seismic sequences, structural elements and geological development. Geologische Jahrbuch E23, 17-41.

Holt, J.W., Richter, T.G., Kempf, S.D., Morse, D.L., 2006. Airborne gravity over Lake Vostok and adjacent highlands of East Antarctica. Geochemistry, Geophysics, Geosystems 7, doi:10.1029/2005GC001177.

Hübscher, C., Jokat, W., Miller, H., 1996. Structure and origin of southern Weddell Sea crust: results and implications, in: Storey, B.C., King, E.C., Livermore, R.A. (Eds.), WeddellSea Tectonics and Gondwana Break-up. Geological Society Special Publication, pp. 201-211.

Hunter, S.J., Johnson, A.C., Aleshkova, N.D., 1996. Aeromagnetic data from the southern Weddell Sea embayment and adjacent areas: synthesis and interpretation, in: Storey, B.C., King, E.C., Livermore, R.A. (Eds.), Weddell Sea Tectonics and Gondwana Break-up. Geological Society Special Publication, pp. 143-154.

ACCEPTED MANUSCRIPT

Hvidegaard, S.M., Sørensen, L.S., Forsberg, R., 2011. ASTER GDEM validation using LiDAR data over coastal regions of Greenland. Remote Sensing Letters 3, 85-91.

Jankowski, E.J., Drewry, D.J., 1981. The structure of West Antarctica from geophysical studies. Nature 291, 17-21.

Jokat, W., Hübscher, C., Meyer, U., Oszkó, L., Schöne, T., Versteeg, W., Miller, H., 1996. The continental margin off East Antarctica between 10°W and 30°W, in: King, E.C., Livermore, R.A. (Eds.), Weddell Sea Tectonics and Gondwana Break-up. Geol. Soc. Spec. Publ.

Jones, P.C., Ferris, J.K., 1999. Short note: A new estimate of the adopted gravity value at Rothera Station, Antarctic Peninsula. Antarctic Science 11, 461-462.

Jones, P.C., Johnson, A.C., von Frese, R.R.B., Corr, H., 2002. Detecting rift basins in the Evans Ice Stream region of West Antarctica using airborne gravity data. Tectonophysics 347, 25-41.

Jordan, T.A., Ferraccioli, F., Corr, H., Robinson, C., Caneva, G., Armadillo, A., Bozzo, E., Frearson, N., 2007. Linking the Wilkes Subglacial Basin, the Transantarctic Mountains, and the Ross Sea with a new airborne gravity survey, in: Bozzo, E., Ferraccioli, F. (Eds.), The Italian–British Antarctic Geophysical and Geological Survey in Northern Victoria Land 2005–06—Towards the International Polar Year 2007–08. Terra Antartica Reports, pp. 37-54.

Jordan, T.A., Ferraccioli, F., Vaughan, D.G., Holt, J.W., Corr, H., Blankenship, D.D., Diehl, T.M., 2010. Aerogravity evidence for major crustal thinning under the Pine Island Glacier region (West Antarctica). Geol. Soc. Am. Bull. 122, 714-726, doi: 710.1130/B26417.26411.

ACCEPTED MANUSCRIPT

Kennedy, S., Cosandier, D., Hamilton, J., 2007. GPS/INS Integration in Real-time and Postprocessing with NovAtel's SPAN System, International Global Navigation Satellite Systems Society Symposium, The University of New South Wales, Sydney, Australia.

Ku, C.C., Sharp, J.A., 1983. Werner deconvolution for automated magnetic interpretation and its refinement using Marquardt inverse modeling. Geophysics 48, 754–774.

LaCoste, L.J.B., 1967. Measurement of gravity at sea and in the air. Reviews of geophysics 5, 477-526.

Lane, R.J.L., 2004. Airborne Gravity 2004 – Abstracts from the ASEG-PESA Airborne Gravity 2004 Workshop. Geoscience Australia Record 2004/18.

Leat, P.T., 2008. On the long distance transport of Ferrar magmas, in: Thomson, K., Petford, N. (Eds.), Structure and Emplacement of High-level Magmatic Systems. Special Publication of the Geological Society, London, pp. 45-61.

Leitchenkov, G.L., Kudryavtzev, G.A., 2000. Structure and origin of the Earth's crust in the Weddell Sea Embayment (beneath the front of the Filchner and Ronne Ice Shelves) from deep seismic sounding data. Polarforschung 67, 143-154.

Leitchenkov, G.L., Miller, H., Zatzepin, E.N., 1996. Structure and Mesozoic evolution of the eastern Weddell Sea, Antarctica: history of early Gondwana break-up, in: Storey, B.C., King, E.C., Livermore, R.A. (Eds.), Weddell Sea Tectonics and Gondwana Break-up. Geological Society, London, Special Publications, pp. 175-190.

Li, Z.X., Li, X.H., Kinny, P.D., Wang, J., Zhang, S., Zhou, H., 2003. Geochronology of Neoproterozoic syn-rift magmatism in the Yangtze Craton, South China and correlations with other continents: evidence for a mantle superplume that broke up Rodinia. Precambrian Research 122, 85-109.

ACCEPTED MANUSCRIPT

Litak, R.K., Brown, L.D., 1989. A modern perspective on the Conrad Discontinuity. EOS Trans AGU 70, 713, doi:710.1029/1089EO00223.

Liu, H., Jezek, K., Li, B., Zhao, Z., 2001. Radarsat Antarctic Mapping Project digital elevation model version 2. National Snow and Ice Data Center, Boulder, Colorado USA, p. Digital media.

Lodolo, E., Menichetti, M., Bartole, R., Ben-Avraham, Z., Tassone, A., Lippai, H., 2003. Magallanes-Fagnano continental transform fault (Tierra del Fuego, southernmost South America). Tectonics 22, doi:10.1029/2003TC001500, 002003.

Lythe, M.B., Vaughan, D.G., BEDMAP-Consortium, 2001. Bedmap: a new ice thickness and subglacial topographic model of Antarctica. Journal of Geophysical Research 106, 11,335-311,351.

Maslanyj, M.P., Damaske, D., 1986. Lessons regarding aeromagnetic surveys during magnetic disturbances in polar regions. British Antarctic Survey Bulletin 73, 9-17.

Maslanyj, M.P., Storey, B.C., 1990. Regional aeromagnetic anomalies in Ellsworth Land: Crustal structure and Mesozoic microplate boundaries within West Antarctica. Tectonics 9, 1515-1532.

Millar, I.L., Pankhurst, R.J., 1987. Rb-Sr geochronology of the region between the Antarctic Peninsula and the Transantarctic Mountains: Haag Nunataks and Mesozoic granitoids, in: McKenzie, G.D. (Ed.), Gondwana Six: Structure, Tectonics, and Geophysics. Geophysical Monograph 40, American Geophysical Union, Washington, D.C., pp. 151-160.

Miller, H.G., Singh, V., 1994. Potential field tilt—a new concept for location of potential field sources. Journal of Applied Geophysicsl Prospecting, 213-217.

ACCEPTED MANUSCRIPT

Minor, D.R., Mukasa, S.B., 1997. Zircon U-Pb and hornblende ^{40}Ar-^{39}Ar ages for the Dufek layered mafic intrusion, Antarctica: Implications for the age of the Ferrar large igneous province. Geochimica et Cosmochimica Acta 61, 2497-2504.

Mushayandebvu, M.F., van Driel, P., Reid, A.B., Fairhead, J.D., 2001. Magnetic source parameters of two-dimensional structures using extended Euler deconvolution. Geophysics 66, 814-823.

Nabighian, M.N., 1972. The Analytic Signal of Two-Dimensional Magnetic Bodies with Polygonal Cross-Section: Its Properties and Use for Automated Anomaly Interpretation. Geophysics 37, 507-517

Pail, R., Goiginger, H., Schuh, W.D., Höck, E., Brockmann, J.M., Fecher, T., Gruber, T., Mayer-Gürr, T., Kusche, J., Jäggi, A., Rieser, D., 2010. Combined satellite gravity field model GOCO01S derived from GOCE and GRACE. Geophysical Research Letters 37, doi:10.1029/2010GL044906.

Parker, R.L., 1973. The rapid calculation of potential anomalies. Geophysical Journal of the Royal Astronomical Society 31, 447-455.

Pilkington, M., Thurston, B.J., 2001. Draping corrections for aeromagnetic data: line versus grid-based approaches. Exploration Geophysics 32, 95–101.

Randall, D.E., MacNiocaill, C., 2004. Cambrian palaeomagnetic data confirm a Natal Embayment location for the Ellsworth-Whitmore Mountains, Antarctica, in Gondwana reconstructions. Geophysical Journal International 157, 105-116.

Reading, H.G., 1980. Characteristics and recognition of strike-slip fault systems, in: Ballance, P.F., Reading, H.G. (Eds.), Sedimentation in oblique-slip mobile zones. Blackwell Scientific Publications, Oxford, pp. 7-26.

ACCEPTED MANUSCRIPT

Reid, A.B., Allsop, J.M., Granser, H., Millet, A.J., Somerton, I.W., 1990. Magnetic interpretation in three dimensions using Euler deconvolution. Geophysics 55, 80-91.

Riley, T.R., Knight, K.B., 2001. Age of pre-break-up Gondwana magmatism. Antarctic Science 13, 99-110.

Ross, N., Bingham, R.G., Corr, H., Ferraccioli, F., Jordan, T.A., Le Brocq, A.M., Rippin, D.M., Young, D.A., Blankenship, D.D., Siegert, M.J., 2012. Steep reverse bed slope at the grounding line of the Weddell Sea sector in West Antarctica. Nature Geoscience, doi: 10.1038/NGEO1468.

Royden, L., Keen, C.E., 1980. Rifting process and thermal evolution of the continental margin of Eastern Canada determined from subsidence curves. Earth and Planetary Science Letters 51, 343-361.

Shepherd, T., Bamber, J.L., Ferraccioli, F., 2006. Subglacial geology in Coats Land, East Antarctica, revealed by airborne magnetics and radar sounding. Earth and Planetary Science Letters 244, 323–335.

Storey, B.C., 1995. The role of mantle plumes in continental breakup: case histories from Gondwanaland. Nature 377, 301-308.

Storey, B.C., Dalziel, I.W.D., 1987. Outline of the structural and tectonic history of the Ellsworth Mountains-Thiel Mountains ridge, West Antarctica, in: McKenzie, G.D. (Ed.), Gondwana Six; Structure, tectonics, and geophysics. AGU Geophysical Monograph, pp. 117-128.

Storey, B.C., Hole, M.J., Pankhurst, R.J., Millar, I.L., Vennum, W., 1988. Middle Jurassic within-plate granites in west Antarctica and their bearing on the break-up of Gondwanaland. Journal of the Geological Society (London) 145, 999-1007.

ACCEPTED MANUSCRIPT

Storey, B.C., Kyle, P.R., 1997. An active mantle mechanism for Gondwana breakup. S. Afr. J. Geol 100, 283-290.

Storey, B.C., Leat, P.T., Ferris, J.K., 2001. The location of mantle plume centres during the initial stages of Gondwana break-up. Geological Society of America Special Paper 352, 71-80.

Storey, B.C., Pankhurst, R.J., Johnson, A.C., 1994. The Grenville Province within Antarctica: a test of the SWEAT hypothesis. Journal of the Geological Society (London) 151, 1-4.

Studinger, M., Bell, R., Finn, C.A., Blankenship, D.D., 2002. Mesozoic and Cenozoic extensional tectonics of the West Antarctic Rift System from high-resolution airborne geophysical mapping. Royal Society of New Zealand Bulletin 35, 563-569.

Studinger, M., Miller, H., 1999. Crustal structure of the Filchner-Ronne shelf and Coats Land, Antarctica, from gravity and magnetic data: Implications for the breakup of Gondwana. Journal of Geophysical Research 104, 20379-20394.

Tack, L., Wingate, M.T.D., Liégeois, J.P., Fernandez-Alonso, M., Deblond, A., 2001. Early Neoproterozoic magmatism (1000–910 Ma) of the Zadinian and Mayumbian Groups (Bas-Congo): onset of Rodinia rifting at the western edge of the Congo craton. Precambrian Research 110, 277-306.

Talwani, M., Ewing, M., 1960. Rapid computation of gravitational attraction of three-dimensional bodies of arbitrary shape. Geophysics 25, 203-225.

Taylor, G.K., 2007. Pluton shapes in the Cornubian Batholith: new perspectives from gravity modelling. Journal of the Geological Society (London) 164, 525-528, doi: 510.1144/0016-76492006-76492104

Telford, W.M., Geldart, L.P., Sheriff, R.E., 1990. Applied Geophysics, 2nd ed. Cambridge University Press, Cambridge.

ACCEPTED MANUSCRIPT

Thiel, E., 1961. Antarctica, one continent or two? Polar Record 10, 335-348.

Vaughan, D.G., Corr, H., Ferraccioli, F., Frearson, N., O'Hare, A., Mach, D., Holt, J.W., 2006. New boundary conditions for the West Antarctic Ice Sheet: subglacial topography beneath Pine Island Glacier. Geophysical Research Letters 33, doi:10.1029/2005GL025588.

Vennum, W., Storey, B.C., 1987a. Correlation of gabbroic and diabasic rocks from the Ellsworth Mountains, Heart Hills, and Thiel Mountains, West Antarctica, in: McKenzie, G.D. (Ed.), Gondwana Six: Structure, Tectonics and Geophysics. Geophysical Union, pp. 129-138.

Vennum, W.R., Gizycki, P., Samsonov, V.V., Markovich, A.G., Pankhurst, R.J., 1992. Igneous petrology and geochemistry of the Southern Heritage Range, Ellsworth Mountains, West Antarctica, in: Webers, G.F., Craddock, C., Splettstoesser, J.F. (Eds.), Geology and Paleontology of the Ellsworth Mountains, West Antarctica: Geological Society of America Memoir, pp. 295-324.

Vennum, W.R., Storey, B.C., 1987b. Petrology, Geochemistry, and Tectonic Setting of Granitic Rocks From the Ellsworth- Whitmore Mountains Crustal Block and Thiel Mountains, West Antarctica, in: McKenzie, G.D. (Ed.), Gondwana Six: Structure, Tectonics and Geophysics. Geophysical Union, Geophys. Monogr, pp. 129-138.

Voss, M., Jokat, W., 2007. Continent–ocean transition and voluminous magmatic underplating derived from P-wave velocity modelling of the East Greenland continental margin. Geophysical Journal International 170, 580–604, doi: 510.1111/j.1365-1246X.2007.03438.x.

White, N., McKenzie, D.P., 1988. Formation of the "steer's head" geometry of sedimentary basins by differential stretching of the crust and mantle. Geology 16, 250-253, doi: 210.1130/0091-7613(1988)1016<0250:FOTSSH>1132.1133.CO;1132.

ACCEPTED MANUSCRIPT

White, R.A., McKenzie, D.P., 1989. Magmatism at rift zones: The generation of volcanic continental margins and flood basalts. Journal of Geophysical Research 94, 7685-7729.

Woollard, G.P., 1979. The new gravity system - Changes in international gravity base values and anomaly values. Geophysics 44, 1352-1366.

Yin, A., Taylor, M.H., 2011. Mechanics of V-shaped conjugate strike-slip faults and the corresponding continuum mode of continental deformation. Geol. Soc. Am. Bull. 123, 1798-1821, doi: 1710.1130/B30159.30151.

Zeng, H., Wan, T., Teyssier, C., Yao, C., Tikoff, B., 2000. The 3-D geometry of the Linglong granitic complex from 2-D gravity forward modeling, Shandong Province, east China. Geophysics 65, 421–425.

ACCEPTED MANUSCRIPT

ACCEPTED MANUSCRIPT

Figure 1. Regional tectonic setting of the Weddell Sea Rift superimposed on bed elevation and bathymetry data from BEDMAP (Lythe et al., 2001) and Bouguer anomaly data (Studinger and Miller, 1999). The grey box marks the ~27 km thick rifted continental crust in the Central Trough (CT) region (Studinger and Miller, 1999). White dashed lines define the main tectonic blocks of West Antarctica (Dalziel and Elliot, 1982): Ellsworth-Whitmore Mountains block (EWM); AP (Antarctic Peninsula); TI (Thurston Island); and MBL (Marie Byrd Land). Red box marks our study area over the inland extent of the Weddell Sea Rift and adjacent EWM. The Explora and Orion magnetic anomalies are outlined in yellow and relate to Jurassic magmatism and rifting in the Weddell Sea Embayment (Hunter et al., 1996). Pink lines mark rift zones (Aleshkova et al., 2000) and include the Filchner Rift (FR) and Weddell Rift Anomaly (WRA). IIS:Institute Ice Stream; MIS:Möller Ice Stream; HN: Haag Nunataks; RIS: Ronne Ice Shelf; BI: Berkner Island; DI: Dufek Intrusion; TT:Thiel Trough; TAM: Transantarctic Mountains.

Figure 2. a) Location of the aerogeophysical survey (magenta) and regional geology overlain on RADARSAT image of the ice surface (Liu et al., 2001). Dashed yellow outline marks inferred margin of EWM block and the dashed white line marks the location of the inferred tectonic boundary between East and West Antarctica (Dalziel and Elliot, 1982). Note the location of the Ellsworth and Marginal domains (Storey and Dalziel, 1987). Age of Jurassic granites shown in white from Storey et al., (1988). Dashed white and black lines in this and subsequent figures depict the location of our magnetic and gravity models. The red box denotes the only available estimate of crustal thickness from seismic data in the survey area (Behrendt et al., 1974). Black dashed lines mark catchment boundaries for the Institute and Möller Ice Streams. b) Aerogeophysical flight lines are shown in red and blue sections mark areas where aerogravity data were recovered. The four survey elevation blocks are shown in

ACCEPTED MANUSCRIPT

yellow. Previous survey lines over West Antarctica (Bell et al., 1998; Vaughan et al., 2006), and East Antarctica (Ferris et al., 2003) are shown in pink. C110 and Patriot Hills (green triangles) mark the two field camps and locations of magnetic base stations.

Figure 3. New subglacial topography and total field aeromagnetic anomaly map. a) Subglacial topography. Solid yellow lines define margins of the Transitional Basins and solid white lines mark edges of the Marginal Basins. Note that the Coastal Basins include the Western and Southern basins. Abbreviations are; PH: Pirrit Hills; NH: Nash Hills; HH: Hart Hills; PN: Pagano Nunatak; SH: Stewart Hills; TM: Thiel Mountains; WM: Whitmore Mountains. Other features as in Figure 2a. b) Reduced To the Pole (RTP) aeromagnetic data. Anomalies M1 and EA (Ellsworth Anomaly) are interpreted as Proterozoic basement and Cambrian igneous rocks respectively. Magnetic anomalies overlie exposed Jurassic granites (PH, NH and PN) and anomalies M2-M6 are interpreted as reflecting buried Jurassic intrusions. L1-L5, and L7 denote major magnetic lineaments. Note Transitional Basins marked as black lines. Red box marks detailed study area in Figures 5-6.

Figure 4. New aerogravity data. a) Free air anomaly map. b) Bouguer anomaly map. Note the contrast between the positive Bouguer anomaly field over the proposed inland extent of the Weddell Sea Rift and the broad low over the thicker crust of the EWM. Shorter wavelength negative Bouguer anomalies generally correspond to positive magnetic anomalies (pink outline) over exposed and buried Jurassic intrusions.

Figure 5. a) Aeromagnetic anomalies upward continued to an elevation of 10 km. The main magnetic anomalies seen in the original total field data are maintained suggesting that thick source bodies are causing the anomalies. b) Residual wavelengths after subtraction of 10 km upward continued field from the RTP anomaly grid. Shorter wavelength anomalies associated

ACCEPTED MANUSCRIPT

with shallower and thinner source bodies are enhanced in this presentation (e.g. anomalies M7 and M8 that are interpreted as reflecting Cambrian igneous rocks).

Figure 6. a) Maximum horizontal gradient of pseudo-gravity with superimposed magnetic lineations in white. b) Tilt derivative magnetic map showing lineaments over anomaly crests. c) Anomaly margins (black outlines) from the normalised maximum horizontal gradient of the tilt derivative (TDX) overlain on subglacial topography. d) Apparent magnetic susceptibility calculated from aeromagnetic anomaly data. White boxes locate maps in Figures 7 and 8.

Figure 7. Depth to source calculations along the inland profile located in Fig. 6. a) Map of 3D Euler solutions (coloured circles) over the Nash Hills region. Background coloured image shows Bouguer gravity anomaly overlain on contoured magnetic anomalies (10 nT contour interval) and anomaly margins from TDX (black outline). Note that the outcrops of weakly magnetic Jurassic granite (pink) lie at the edges of the magnetic anomalies (see Section 8.3 for discussion). Solid black line marks the trace of the 2D depth to source profile. b) Same as above over the Pagano Anomaly region. Jurassic granites at Pagano Nunatak (PN) lie at the margin of the anomaly. Note the deeper estimated source depths for the Pagano Anomaly compared to the Nash Hills region and the location of quartz-gabbro rocks (red) at Hart Hills (HH). c) Profile of magnetic anomaly (black), and 2D horizontal (dh) and vertical (dz) derivatives of the magnetic field (grey). d) Ice surface (grey) and subglacial topography (black). e) Depth to source solutions for contact and dyke bodies from 2D Analytical Signal (blue) and Werner Deconvolution (red) are shown as circles and diamonds respectively. Note the shallow clusters of solutions over the Jurassic granites of the Nash Hills region and the paucity of solutions over the Transitional Basins indicative of weakly magnetic

ACCEPTED MANUSCRIPT

metasediments and/or sediments. f) 2D Extended Euler solutions for structural index 0 (contact and large throw fault) and 1 (dyke and low-throw fault) are shown in magenta and orange respectively. Note the deeper clusters obtained for the Nash Hills and Pagano Anomaly in the dyke model.

Figure 8. Depth to magnetic source calculations across the Coastal Basins (outlined in white). a) 3D Euler solutions (coloured dots). Background colour image shows the Bouguer gravity anomalies overlain on the contoured magnetic anomalies (10 nT contour interval) and anomaly margins from TDX (black outline). Solid black line marks 2D profile. b) Magnetic anomaly (black), and horizontal (dh) and vertical (dz) derivatives of the magnetic field (grey). Note the higher amplitude magnetic anomaly M1 attributed to Proterozoic basement and anomaly M3 interpreted as reflecting Jurassic intrusions flanking the Coastal Basins and the quiet magnetic pattern within the basins. Also note the position of magnetic lineaments L3 and L4. c) Ice surface (grey) and subglacial topography (black). d) Depth to source solutions for contact and dyke bodies from 2D Analytical Signal (blue) and Werner Deconvolution (red) are shown as circles and diamonds respectively. Two clusters of shallow source solutions within Coastal Basins are used to help constrain potential sedimentary thickness within the basins. e) 2D Extended Euler solutions for structural index 0 (contact and large throw fault) and 1 (dyke and low-throw fault) are shown in magenta and orange respectively. Shallower solutions within the Coastal Basins are not apparent from Extended Euler estimates but deeper solutions are consistent with previous models for over 10 km thick metasediments overlying magnetic Proterozoic basement (Maslanyj et al., 1990).

Figure 9. 2D forward magnetic and gravity models. a) Inland crustal model crossing Nash Hills and the Pagano Anomaly. Panel 1 shows observed and calculated aeromagnetic

ACCEPTED MANUSCRIPT

anomalies (dashed grey and black lines respectively). Solid grey line shows residual error. Panel 2 shows observed and calculated Bouguer gravity anomaly (grey dashed and solid lines respectively). Solid grey line shows residual error. Panel 3 shows model crustal structure and depth to source solutions. Light grey circles=Werner Deconvolution solutions and Triangles=Analytical Signal solutions. Dark grey and black solutions mark Extended Euler Deconvolution results for 5 and 20 km windows. The starting model included upper crust (light grey), lower crust (intermediate) and mantle (dark grey) interfaces. Magnetic susceptibility and densities of the bodies are set out in Table 2. The positive magnetic anomalies and negative Bouguer gravity anomalies (B2-B4) are modelled as reflecting 5-8 km thick Jurassic intrusions (I1-I5). Note the thin sediments modelled beneath the Transitional Basins (S). The long-wavelength Bouguer anomaly high (B1) over the Transitional Basins is modelled as arising from ~3 km of crustal thinning beneath the basins. (b) Crustal model across the Coastal Basins. Panels as in (a). Magnetic anomaly M1 is modelled as arising from >10 km thick Proterozoic basement (C1) and M3 as arising from a thin Jurassic intrusion (C2). The thickness of the inferred sedimentary infill in the Coastal Basins (S) is constrained from Werner solutions and gravity modelling (anomaly B5) as ~2 km thick. Note ~4 km of crustal thinning beneath the Coastal Basins interpreted as reflecting the inland continuation of the Weddell Sea Rift.

Figure 10. Alternative models for the inland and coastal profiles incorporating magmatic underplating beneath the Jurassic intrusions. Other features as in Figure 9.

Figure 11. a) Interpreted magnetic lineations are shown in magenta and overlain on Radarsat image, geology and structural domains (Blue=Ellsworth Domain; Red= Marginal Domain; Orange=East Antarctica). Yellow lines mark edges of main magnetic anomalies (labels as in

ACCEPTED MANUSCRIPT

previous figures). Black lines denote the Transitional Basins and green shaded area shows inferred sediments in the Coastal Basins. White boxes denote the location of the detailed views shown in figures 12 and 13. b) Rose diagrams for magnetic lineations and strain ellipse. b1. All magnetic lineations for the study area within a 5 degree bin. Note that the data are plotted relative to the 80° W (N-S) axis. b2. Magnetic lineations within the Ellsworth Domain revealing a dominant ESE-WNW orientation. b3. Magnetic lineations within the Marginal Domain interpreted as predominantly reflecting the Pagano Shear Zone, a major left-lateral strike-slip fault zone (see also b4). Note that the ~E-W trends are interpreted as left-lateral P shear zones and the ENE-WSW trends are inferred to represent subsidiary synthetic shear zones (SS). Other ~N-S and NE-SW trends are less clear but may reflect antithetic shear zones and normal faults respectively. b4. Strain ellipse for a left-lateral strike slip fault system and orientation of fault patterns with respect to the Principal Displacement Zone (PDZ). (Lodolo et al., 2003). c) New geological sketch map derived from magnetic and gravity interpretation overlain on the Radarsat image. The left-lateral Pagano Shear Zone (magenta area) is interpreted as forming the tectonic boundary between the Marginal and Ellsworth domains and is marked by major magnetic lineations (L2-L5). The thin black lines denote the en-echelon Transitional Basins inferred to be structurally controlled and related to the Pagano Shear Zone. Note in the Western Basin region the thick black line (L7) interpreted as a rift-related fault that flanks a Proterozoic horst-block (M1). The inferred fault is aligned to rift fabric in the Weddell Sea Rift as shown in figure 14. In the Southern Basin region magnetic lineament L3 is interpreted as the margin of the Pagano Shear Zone, which is inferred to control the location of elongated Jurassic intrusions. More circular Jurassic intrusions are also delineated over the EWM and within the shear zone. The inferred post-Jurassic(?) sedimentary infill in the Coastal Basins region is also shown.

ACCEPTED MANUSCRIPT

Figure 12. Detailed view of the Transitional Basins within the Pagano Shear Zone. a) Subglacial topography map and TDX magnetic anomaly margins (black) used to assess structural controls on the en-echelon basins. Colour scale as in Figure 3a. White lines mark locations of profile below. b) Magnetic anomaly map and TDX anomaly margins. Colour scale as in Figure. 3b. E-W oriented magnetic anomaly margins are interpreted as reflecting P shear zones. The ENE-WSW trends are inferred to represent subsidiary synthetic shear zones (SS) and the NE-SW trends are interpreted as normal faults (N). c) Profile view of the magnetic anomalies. Vertical black lines mark margins of the Pagano Anomaly (PA) and anomaly M2. d) Bouguer anomalies. Note negative values over the flanks of the Transitional Basins interpreted as reflecting lower density granitic Jurassic intrusions. e) Maximum horizontal gradient of pseudo–gravity showing clear peaks over the margins of the Pagano Anomaly interpreted as reflecting the P shear zones. f). The tilt derivative (green) enhances magnetic anomaly M2 and high frequency anomalies within the Transitional Basins. The TDX profile enables identification of inferred normal faults (N) and synthetic shear zones (SS). g) Subglacial topography profile showing ~1.2 km of relief between the bed of the Transitional Basins and its flanks. Several magnetic lineations are used to locate inferred faults associated with the ridges and sub-basins within the Transitional Basins. The crosses denote the inferred Jurassic granitic intrusions that cause the magnetic anomalies.

Figure 13. Detailed view of the Coastal Basins. a) Subglacial topography map and TDX magnetic anomaly margins (black) used to assess structural controls on the Western and Southern basins. Colour scale as in Figure 3a. Red lines mark locations of profiles below. b) Magnetic anomaly map and TDX anomaly margins. Colour scale as in Figure. 3b. The ~N-S oriented magnetic lineament L7 is ~ on strike with rift fabric in the Weddell Sea and lies ~orthogonal to the EWM structural grain (e.g. magnetic lineament L1 and EA anomalies in

ACCEPTED MANUSCRIPT

figure 11a). The ~E-W magnetic grain along the flanks of anomaly M3 (magnetic lineaments L3 and L4) lie on strike with the Pagano Shear Zone. c) Magnetic anomalies along profiles P1 (left panel) and P2 (right panel). Note the higher amplitude anomaly (M1) over the inferred Proterozoic basement high and the lower amplitude anomaly M3 over buried Jurassic intrusions. d) Bouguer anomalies. Note the higher values over the Proterozoic basement high and the lower values over the inferred post-rift sedimentary rocks within the Coastal Basins (left panel). A Bouguer anomaly low on the flank of the Southern Basin correlates with magnetic anomaly M3. e) Maximum horizontal gradient of pseudo–gravity. f) The tilt derivative (green) enhances magnetic anomalies M1 and M3. The TDX profiles locate magnetic lineaments L7, L3 and L4 and help guide the interpretation of the extent of the inferred sedimentary basin. g) Subglacial topography revealing the smooth bed over the inferred sedimentary basin (green) and rougher bed over the proposed Proterozoic basement high and Jurassic intrusions (X and + symbols respectively).

Figure 14. Compilation of geophysical data over the Weddell Sea Rift region. a) Bouguer anomaly map revealing the rifted continental crust of the Weddell Sea Rift (green to light blue colours) and the thicker crust of the EWM (purple colours). The black rectangle in panels a, b and c marks our aerogeophysical survey area. Note that the broad Bouguer anomaly high we identified over the Coastal Basins (CB) region is interpreted as revealing the inland extent of the Weddell Sea Rift. The dashed white line denotes the inferred continuation of the Weddell Rift Anomaly (WRA) (Aleshkova et al., 2000). The Bouguer high over the West Antarctic Rift System (WARS) abuts against the EWM. b) Bouguer anomaly map derived from satellite gravity data (Pail et al., 2010) showing the extent of thick crust of the EWM and East Antarctica. The sharp ~E-W oriented boundary between the thicker crust of East Antarctica and the thinner rifted crust within the Weddell Sea Rift (black

ACCEPTED MANUSCRIPT

and white line) is approximately parallel to the newly identified Pagano Shear Zone. A similar sharp transition in crustal thickness was identified from a single oversnow gravity traverse- small and large crosses denote thinner and thicker crust respectively from Behrendt et al., (1974)-. c) Merged aeromagnetic anomaly map including our new survey data, ADMAP (Golynsky et al., 2001) and data over the Dufek Intrusion (Ferris et al., 2003). Note the inferred N-S trending fault (L7) flanking the interpreted Proterozoic horst block in the Coastal Basins region (M1) that lies on strike with rift fabric in the Weddell Sea Rift and the E-W trending Pagano Shear Zone (PSZ) (red line). EA Explora Anomaly, BI, Berkner Island, DI Dufek Intrusion. d) Interpretation map overlain on subglacial topography (grey) from BEDMAP and our new survey. Coloured zones mark magnetic domains within the Weddell Sea Rift region adapted from Golynsky et al., (2000). These include the Proterozoic Haag Domain, the Ronne Domain (interpreted either as Jurassic intrusions and/or rifted basement blocks) and the East Antarctic Margin Domain (that includes Jurassic seaward dipping reflectors and exposed and inferred Jurassic intrusions). Note the newly proposed left-lateral Pagano Shear Zone (PSZ) and the previously inferred right-lateral strike slip fault at the edge of the Dufek intrusion (Support Force Lineament of Ferris et al., 1998). Red rectangle locates detailed views of these proposed strike slip fault systems (figures 15 and 16).

Figure 15. Detailed views of the proposed strike-slip fault systems at the southern end of the Weddell Sea Rift. a) Magnetic interpretation overlain on subglacial topography. Note magnetic lineaments L3-L5 flanking the Pagano Shear Zone (PSZ) and the abrupt termination of the Filchner Rift (FR) along the Support Force Lineament (SFL) shown in red. White lines denote previously proposed left-lateral strike-slip faults and normal faults between Berkner Island (BI) and the Dufek (DI) and Forrestal intrusions (FI) adapted from Ferris et al., (1998).

ACCEPTED MANUSCRIPT

Note that the Thiel Trough (TT) and the inferred normal faults therein lie on strike with the newly identified Pagano Shear Zone. Yellow and green and purple outlines as in Figure 14. b) Same as above but overlain on Aeromagnetic anomaly map.

Figure 16. Alternative kinematic interpretations for the southern end of the Weddell Sea Rift. a) Simple shear model predicting that ~E-W oriented extension within the Weddell Sea Rift is accomodated by left-lateral strike-slip motion on the Pagano Shear Zone. The model predicts westward motion of the EWM (large white arrow) with respect to East Antarctica. FR: Filchner Rift; TT: Thiel Trough. b) Pure shear model with the Pagano Shear Zone (PSZ) and Support Force Lineament (SFL) representing conjugate dextral and sinistral fault systems. The model predicts NW-SE oriented extension in the Weddell Sea Rift and NE-SW oriented compression in the hinge zone between the strike-slip fault systems.

ACCEPTED MANUSCRIPT

ACCEPTED MANUSCRIPT

Table 1. Susceptibility measurements for the Ellsworth Whitmore Mountains crustal block from data held at the Polar Rock Repository at Byrd Polar Research Center, Ohio State University.

	Rock type	Age	Average $x10^{-3}$ SI	Min $x10^{-3}$ SI	Max $x10^{-3}$ SI	Number of records
Haag Nunataks	Fine grained granite and aplite.	Proterozoic	10.42	2.99	15.38	4
Ellsworth Mountains	Igneous rocks.	Cambrian	1.67	0.19	11.9	16
Pirrit Hills	Granite	Jurassic	1.51	0.002	4.9	46
Pagano Nunatak	Granite	Jurassic	0.26	0.05	1.07	12
Nash Hills	Granite	Jurassic	0.89	0.05	2.97	9

ACCEPTED MANUSCRIPT

ACCEPTED MANUSCRIPT

Table 2. Body properties used in object orientated models. Bodies I1-I4 refer to the inland profile (Fig. 10), and bodies C1 and C2 refer to the coastal profile (Fig. 11).

Body	Modelled magnetic anomaly	Magnetic susceptibility $x10^{-3}$ SI	Rock Density kgm^{-3}
UC (Upper crust)		0	2670
LC (lower crust)		0	2950
Mantle		0	3330
S (Sediment)		0	2500
Underplate		0	3100
I1	Nash Hills	7.6	2550
I2	M5	6.3	2550
I3	M4	10	2550
I4	Pagano Nunatak	19.5	2550
I5	Pagano Nunatak/M4	0	2550
C1	M1	17.5	2700
C2	M3	6	2550

ACCEPTED MANUSCRIPT

ACCEPTED MANUSCRIPT

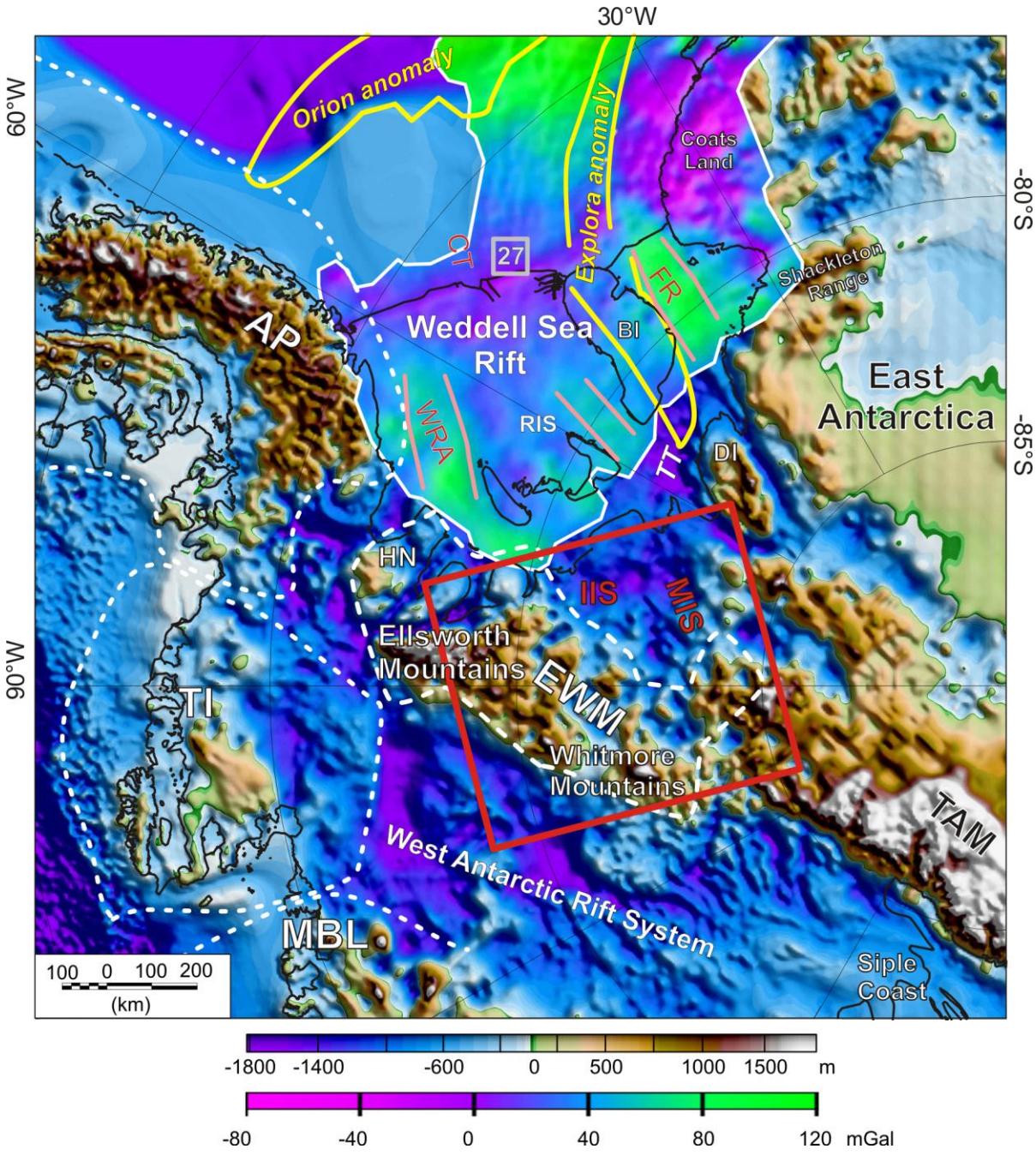

Figure 1

ACCEPTED MANUSCRIPT

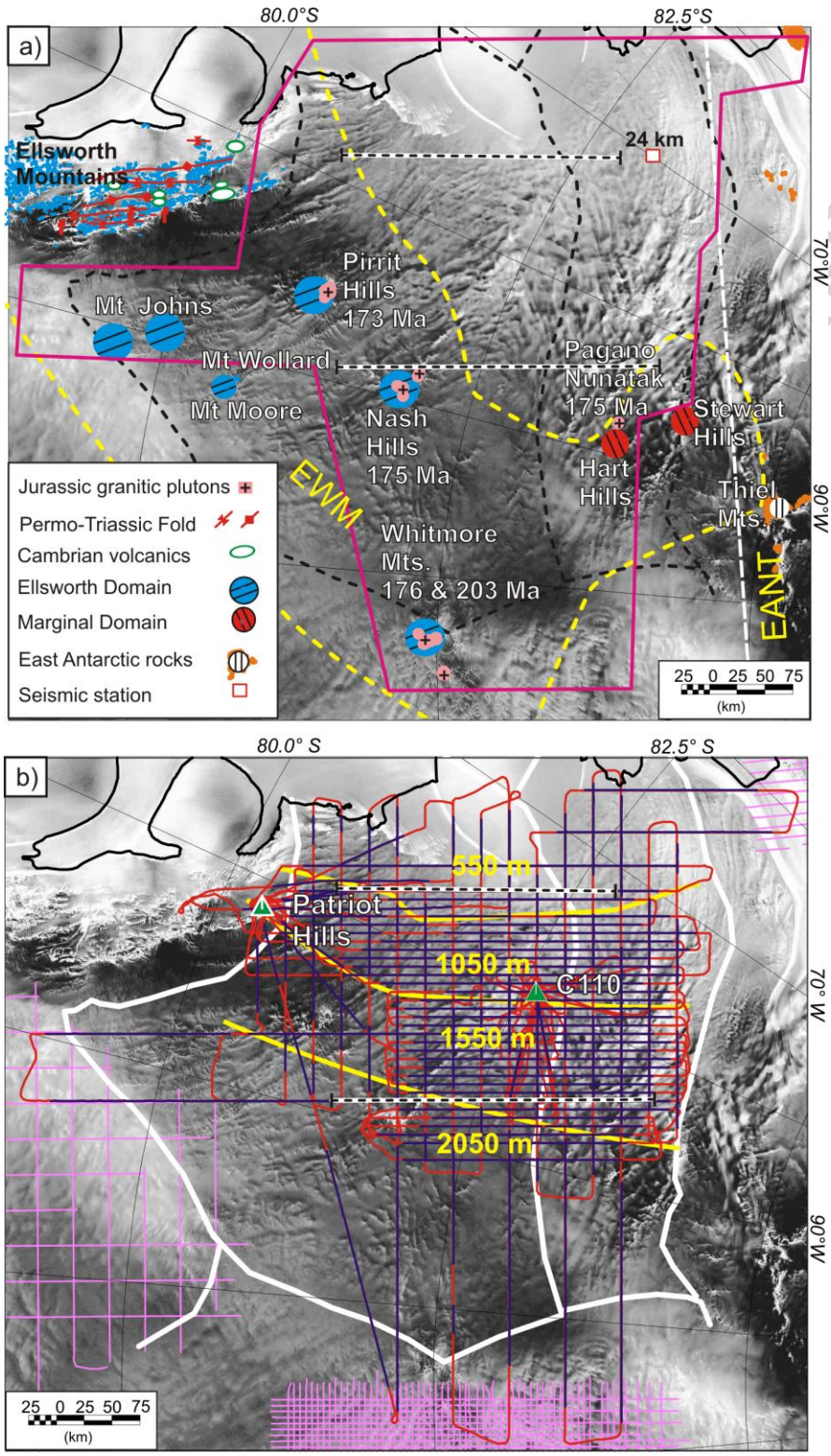

Figure 2

ACCEPTED MANUSCRIPT

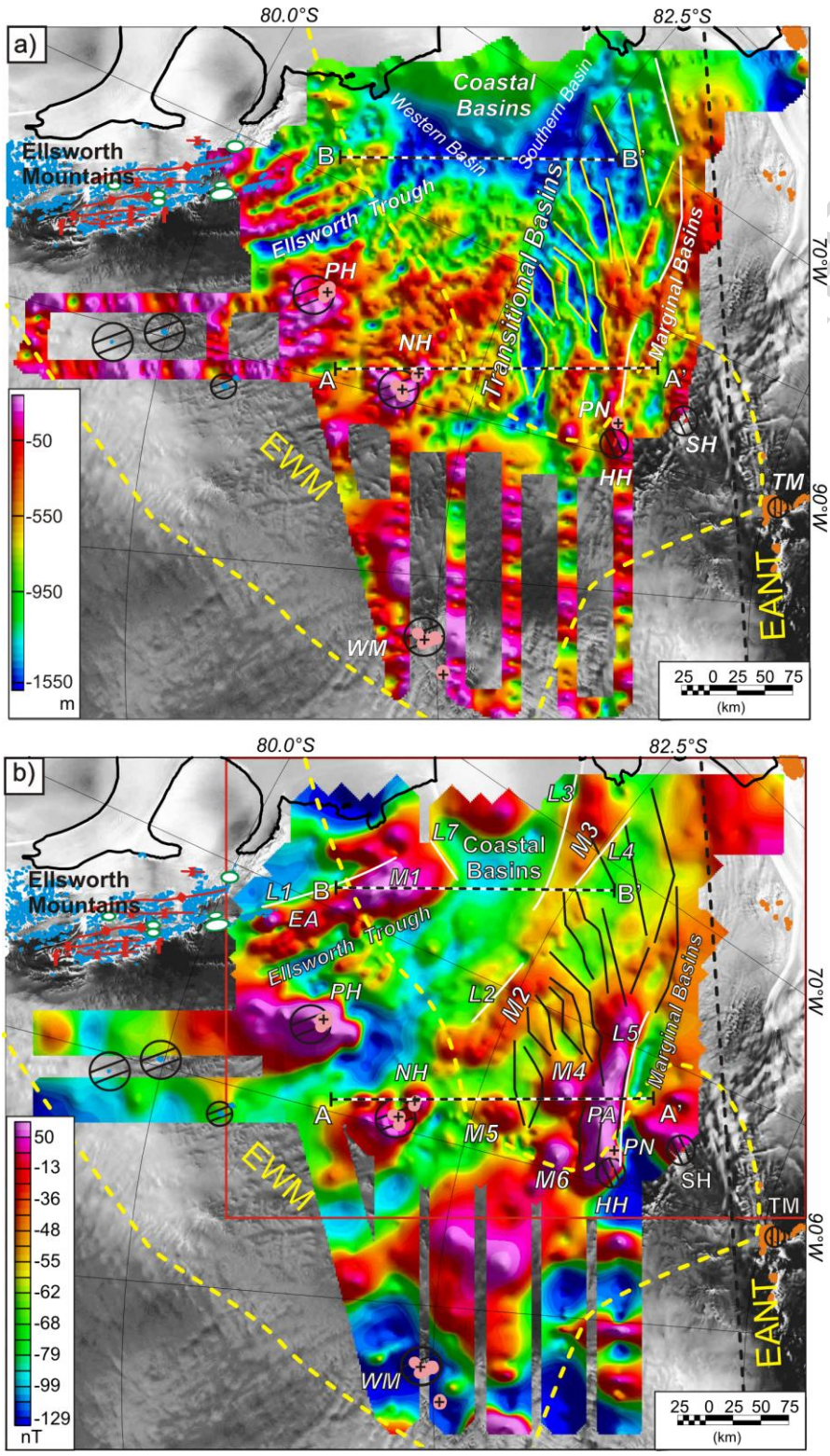

Figure 3

ACCEPTED MANUSCRIPT

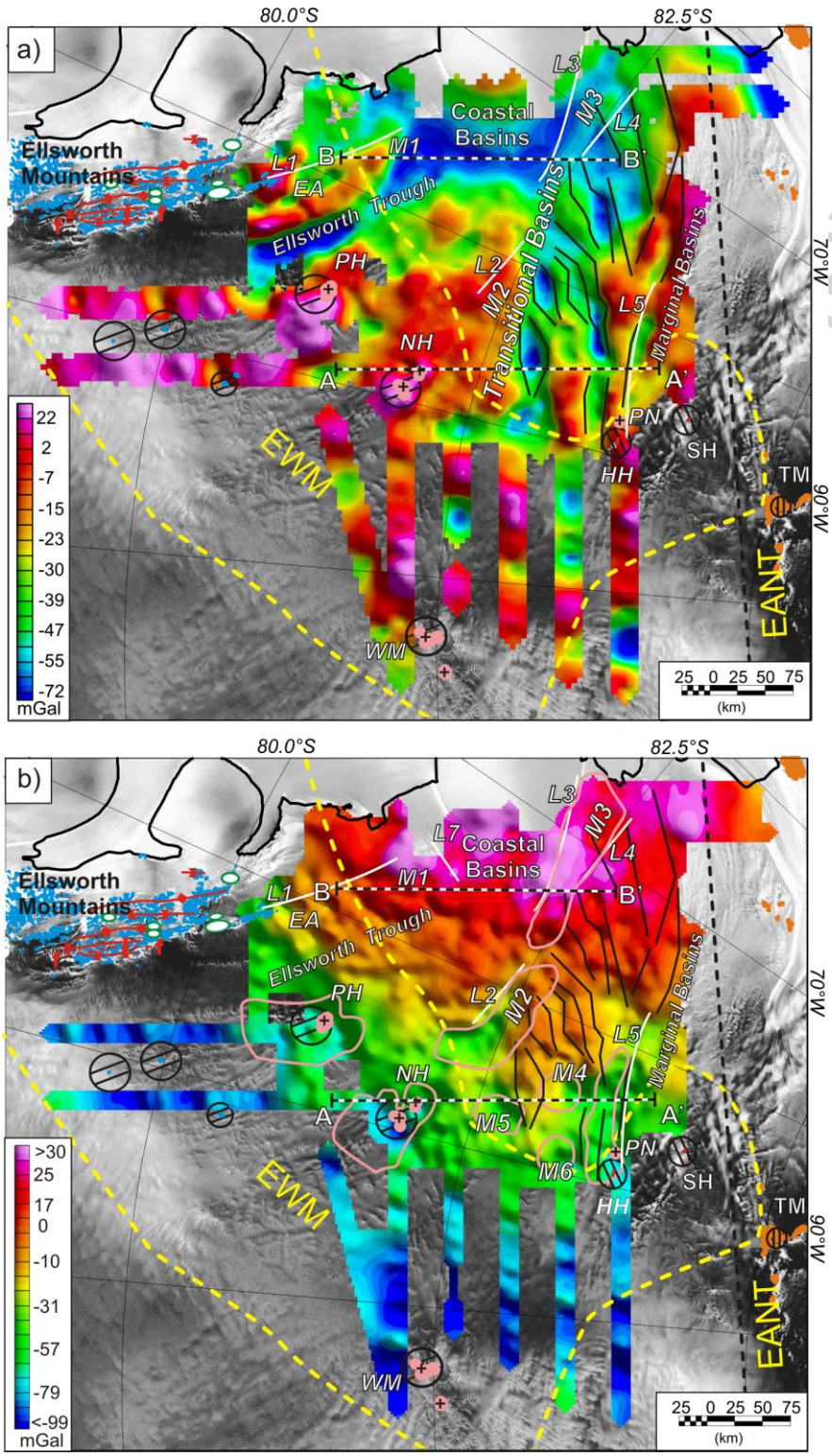

Figure 4

ACCEPTED MANUSCRIPT

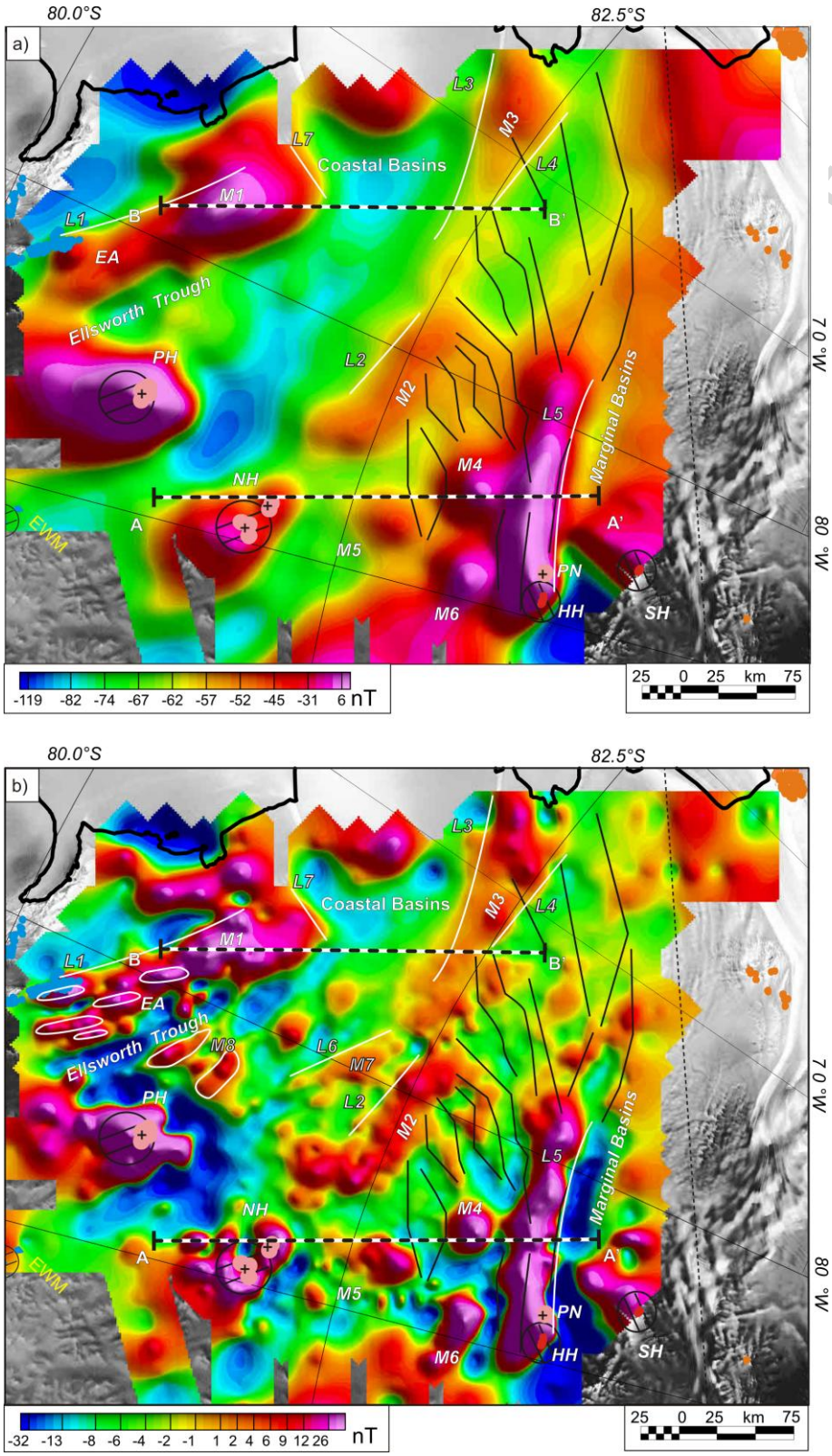

Figure 5

ACCEPTED MANUSCRIPT

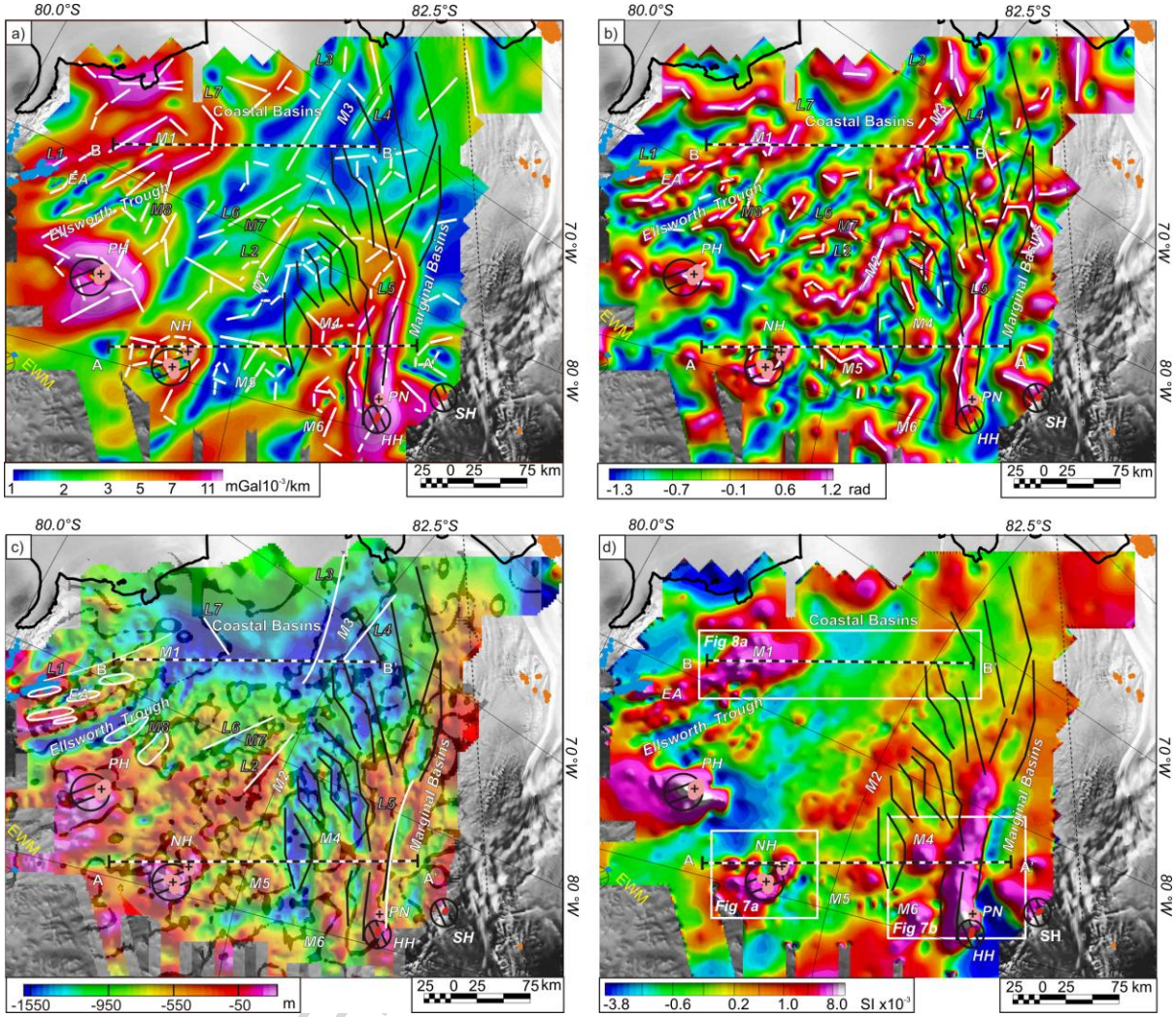

Figure 6

ACCEPTED MANUSCRIPT

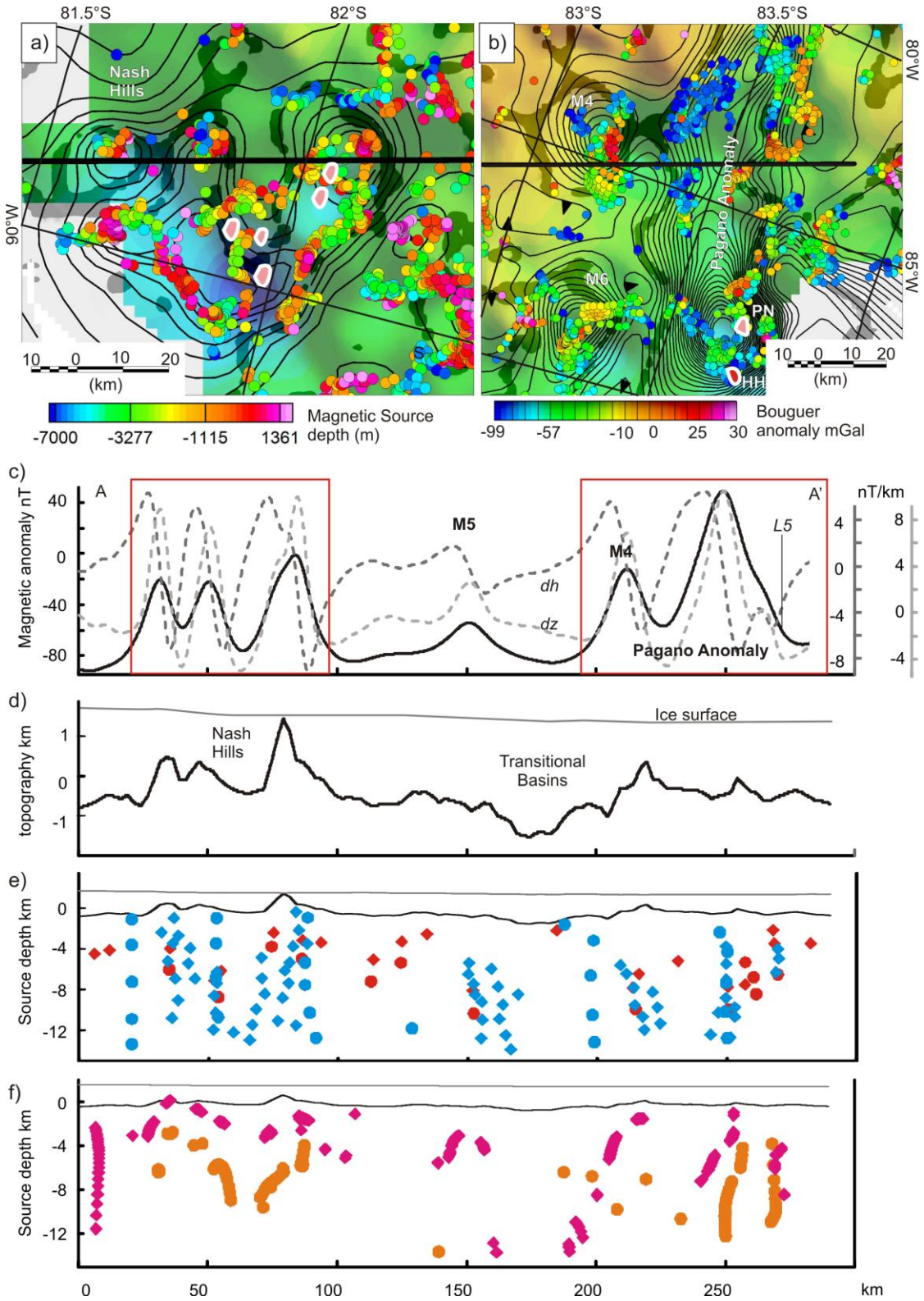

Figure 7

ACCEPTED MANUSCRIPT

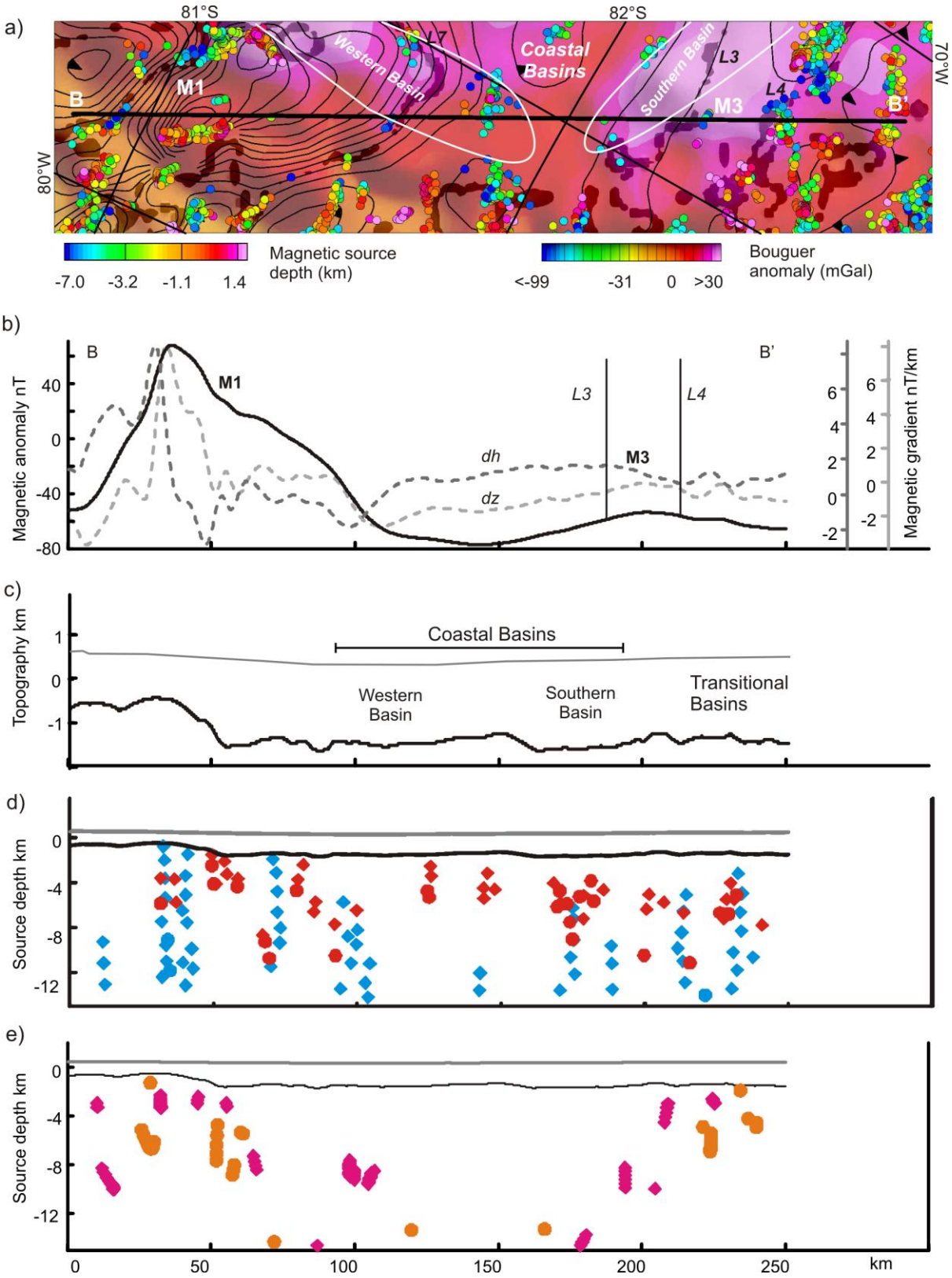

Figure 8

ACCEPTED MANUSCRIPT

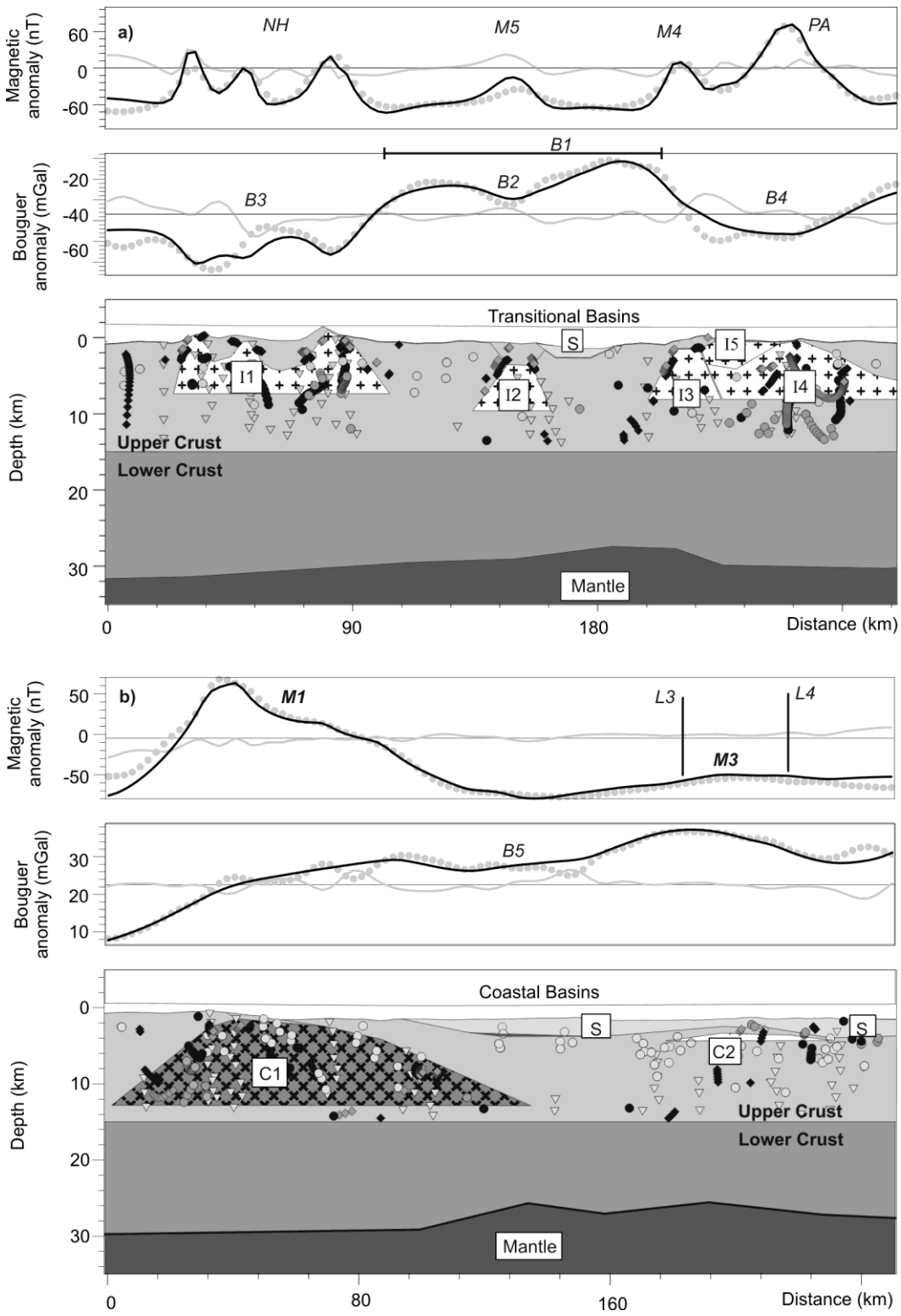

Figure 9

ACCEPTED MANUSCRIPT

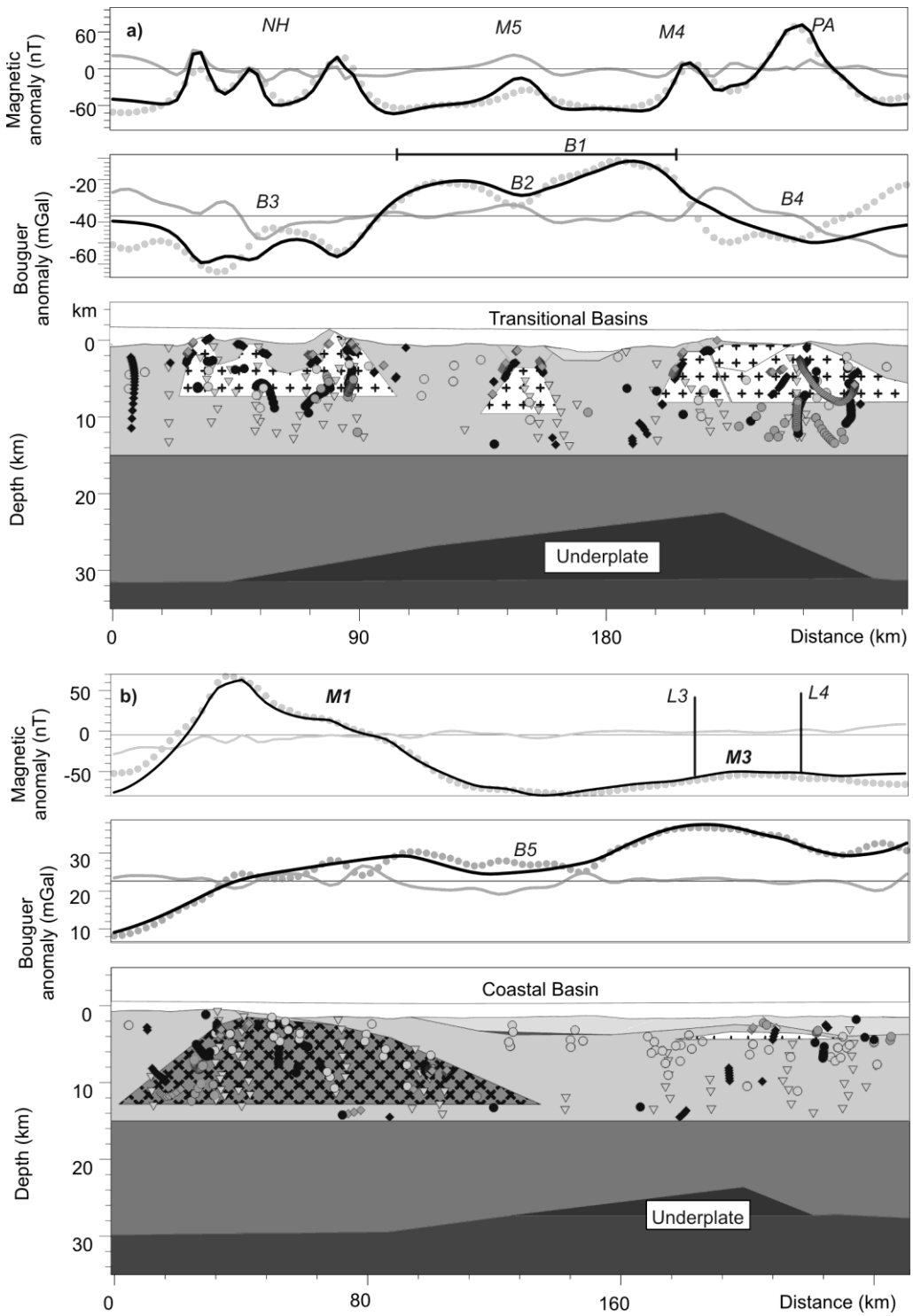

Figure 10

ACCEPTED MANUSCRIPT

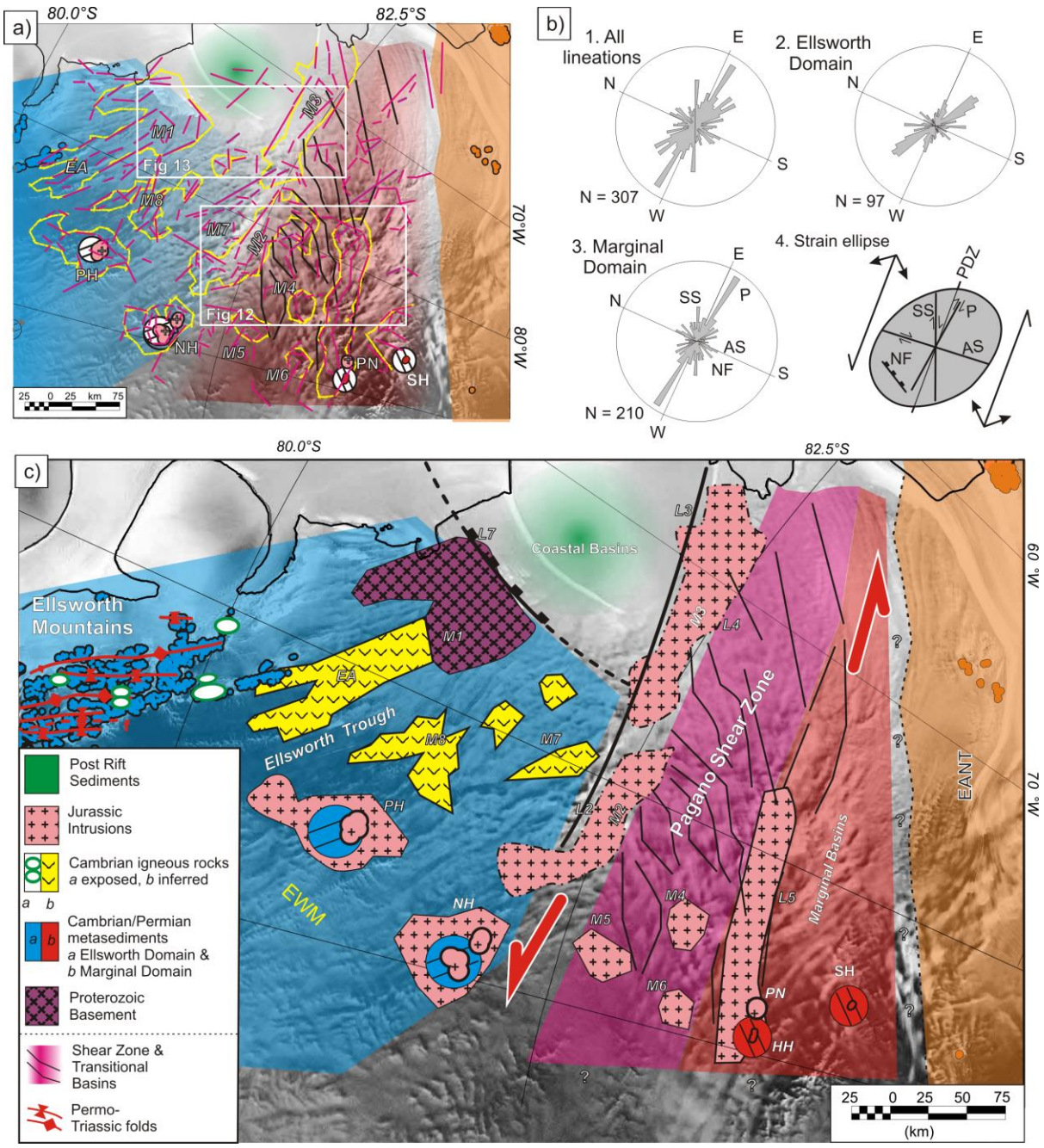

Figure 11

ACCEPTED MANUSCRIPT

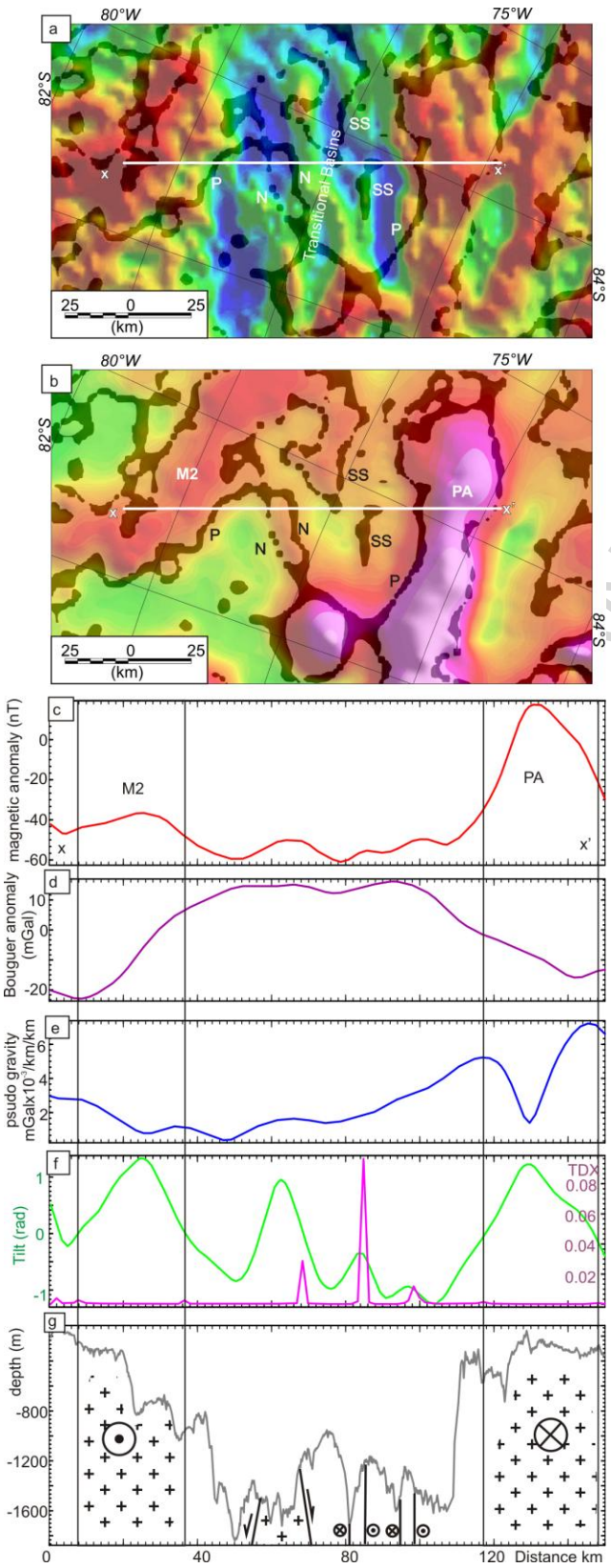

Figure 12

ACCEPTED MANUSCRIPT

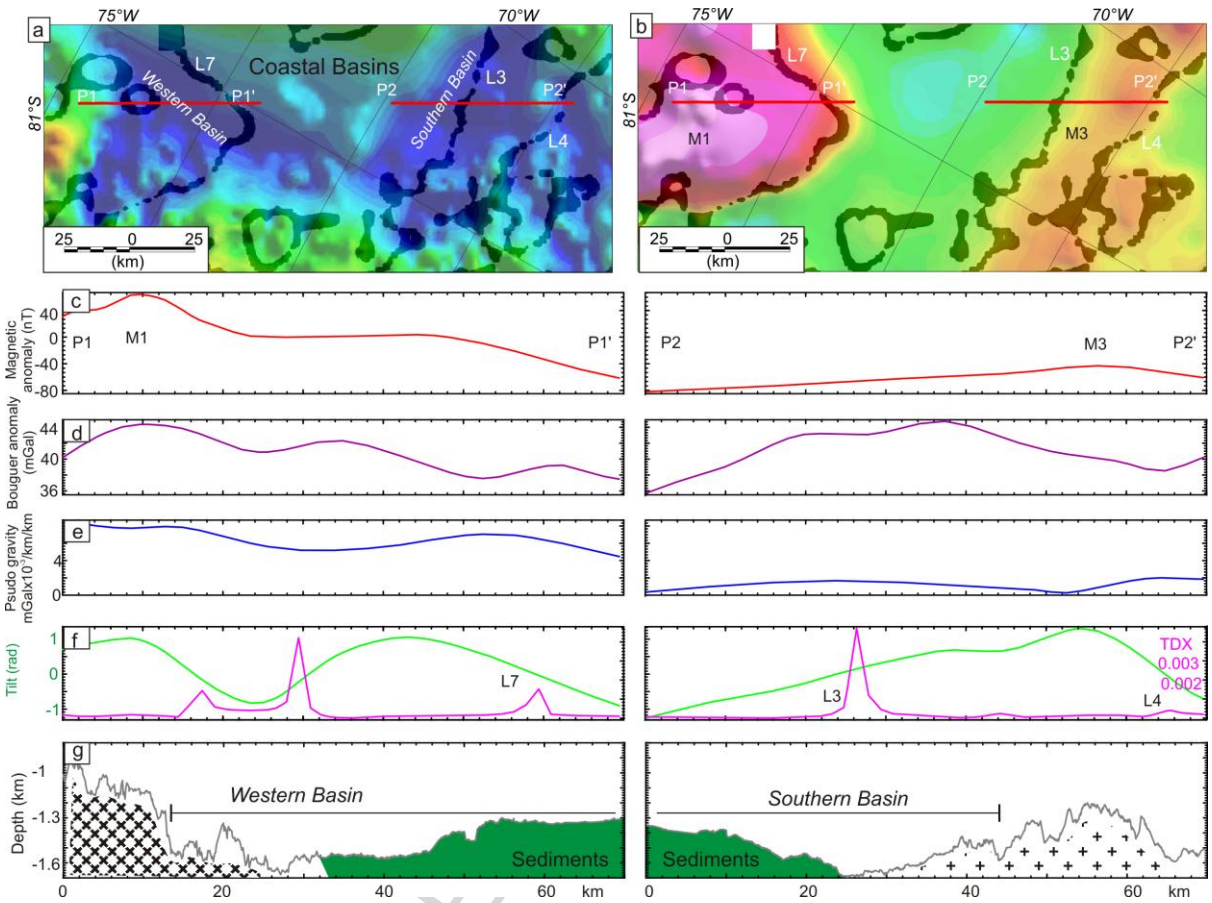

Figure 13

ACCEPTED MANUSCRIPT

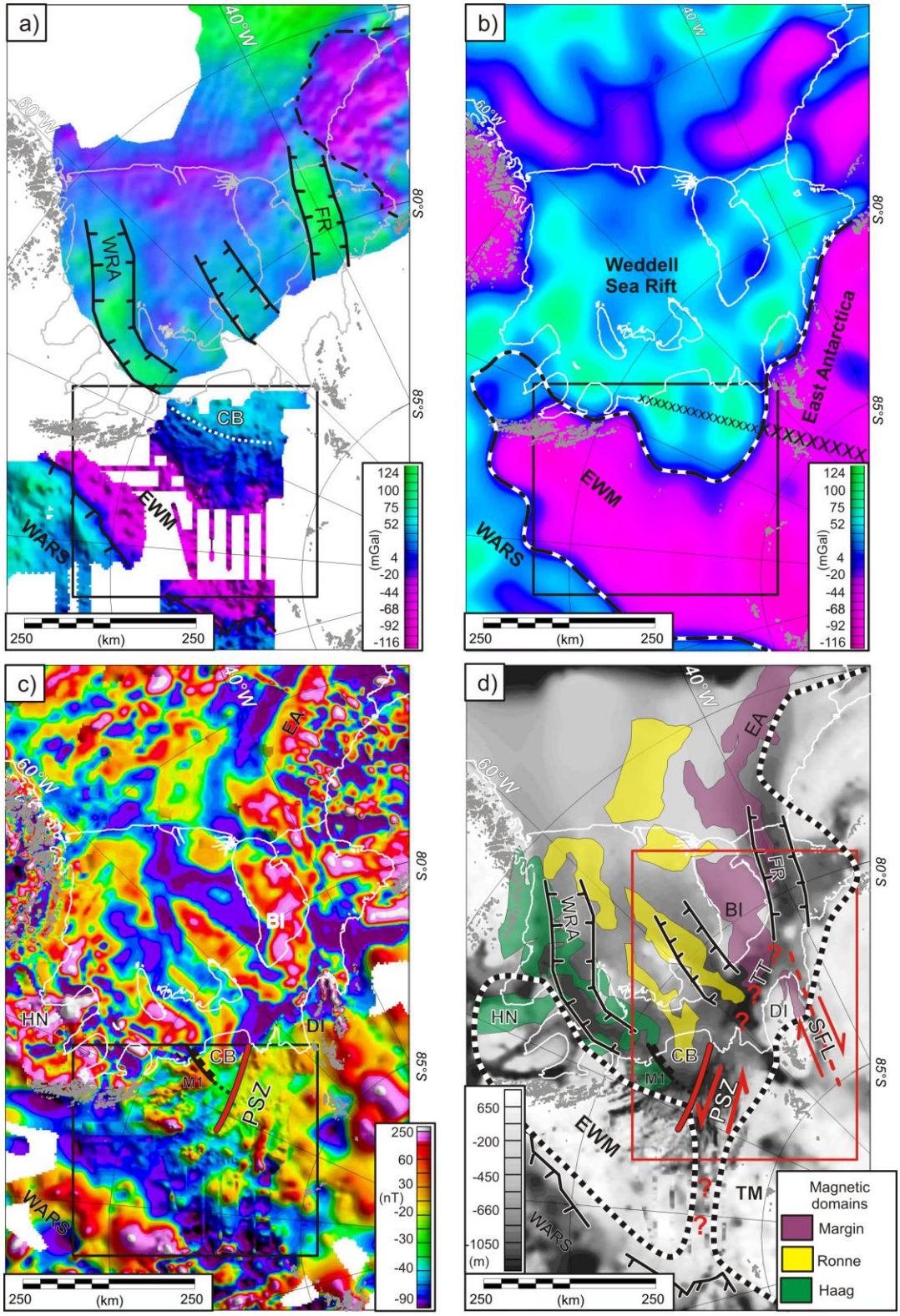

Figure 14

ACCEPTED MANUSCRIPT

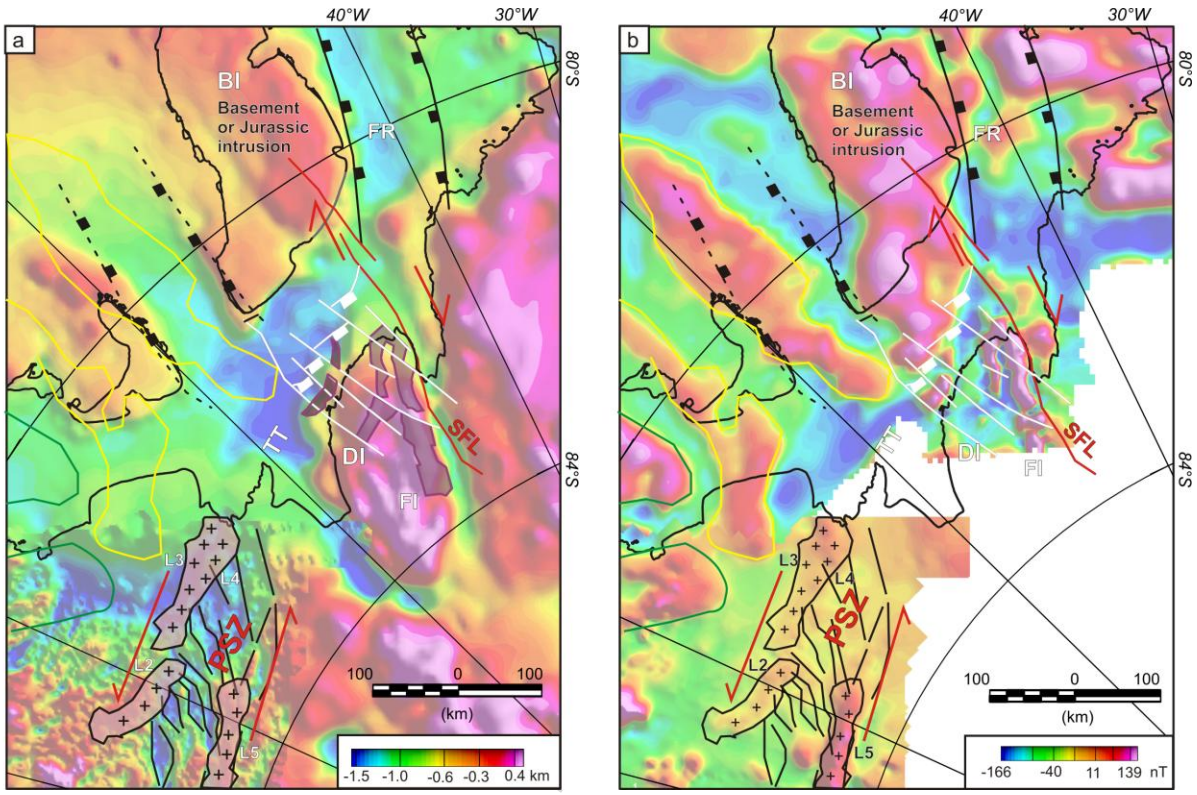

Figure 15

ACCEPTED

ACCEPTED MANUSCRIPT

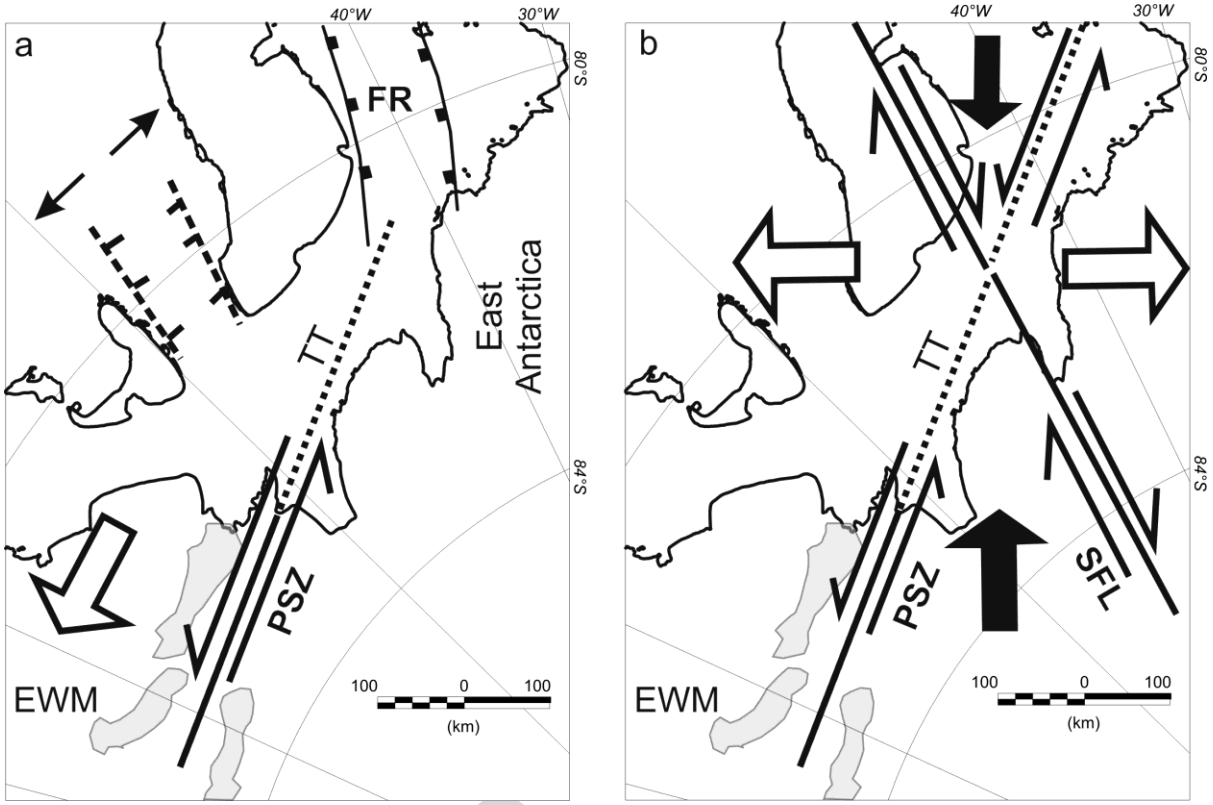

Figure 16

ACCEPTED